Pereira, R., Hitzeroth, I.I., Rybicki, E.P., 2009. Insights into the role and function of L2, the minor capsid protein of papillomaviruses. Arch. Virol. 154, 187–197.
Sapp, M., Selinka, H.C., 2005. Pseudovirions as specific tools for investigation of virus interactions with cells. Methods Mol. Biol. 292, 197–212.
Sokolowski, M., Tan, W., Jellne, M., Schwartz, S., 1998. mRNA instability elements in the human papillomavirus type 16 L2 coding region. J. Virol. 72, 1504–1515.
Stauffer, Y., Raj, K., Masternak, K., Beard, P., 1998. Infectious human papillomavirus type18 pseudovirions. J. Mol. Biol. 283, 529–536.
Sun, X.Y., Frazer, I., Müller, M., Gissmann, L., Zhou, J., 1995. Sequences required for the nuclear targeting and accumulation of human papillomavirus type 6B L2 protein. Virology 213, 321–327.
Unckell, F., Streeck, R.E., Sapp, M., 1997. Generation and neutralization of pseudovirions of human papillomavirus type33. J. Virol. 71, 2934–2939.
Zhou, J., Doorbar, J., Sun, X.Y., Crawford, L.V., McLean, C.S., Frazer, I.H., 1991. Identification of the nuclear localization signal of human papillomavirus type 16 L1 protein. Virology 185, 625–632.

Biochemical and Biophysical Research Communications 387 (2009) 525–530

Contents lists available at ScienceDirect

Biochemical and Biophysical Research Communications

journal homepage: www.elsevier.com/locate/ybbrc

Identification of nucleolin as a protein that binds to human papillomavirus type 16 DNA

Hidetaka Sato [a,b], Rika Kusumoto-Matsuo [a], Yoshiyuki Ishii [a], Seiichiro Mori [a], Tomomi Nakahara [a], Fumiko Shinkai-Ouchi [c], Kei Kawana [b], Tomoyuki Fujii [b], Yuji Taketani [b], Tadahito Kanda [a], Iwao Kukimoto [a,*]

[a] Pathogen Genomics Center, National Institute of Infectious Diseases, 1-23-1 Toyama, Shinjuku-ku, Tokyo 162-8640, Japan
[b] Department of Obstetrics and Gynecology, Faculty of Medicine, University of Tokyo, 7-3-1 Hongo, Bunkyo-ku, Tokyo 113-0033, Japan
[c] Department of Biochemistry and Cell Biology, National Institute of Infectious Diseases, 1-23-1 Toyama, Shinjuku-ku, Tokyo 162-8640, Japan

ARTICLE INFO

Article history:
Received 25 June 2009
Available online 16 July 2009

Keywords:
Human papillomavirus
Nucleolin
Host factor
Genome maintenance

ABSTRACT

Transcription, replication, and segregation of human papillomaviruses (HPVs) are regulated by various host factors, but our understanding of host proteins that bind to the HPV genome is limited. Here we report the results of a search of cellular proteins that can associate with specific genomic regions of HPV type 16 (HPV16). We found that human nucleolin, an abundant nucleolar protein, was preferentially captured *in vitro* by an HPV16 genomic fragment from nucleotide positions (nt) 531–780. Electrophoretic mobility shift assays with a bacterially expressed nucleolin revealed that nucleolin bound to an HPV16 genomic region between nt 604 and 614 in a sequence-dependent manner. Chromatin immunoprecipitation analysis showed that both exogenous and endogenous nucleolin bound to a plasmid containing the HPV16 genomic region in HeLa cells. Furthermore, nucleolin associated with the HPV16 genome stably maintained in HPV16-infected W12 cells, suggesting that the nucleolin binding may be involved in the dynamics of the HPV genome in cells.

Introduction

Human papillomaviruses (HPVs), which are recognized as the causative agents of cervical cancer, have circular double-stranded DNA genomes with sizes close to 8 kbp [1]. HPV infects basal cells in the epidermis and its genome is maintained as episomes, whereas the viral genome amplification occurs in upper differentiating epithelium [2]. Due to the limited coding capacity of its small genome, HPV relies heavily on the function of host cell proteins for viral transcription, replication and segregation [3,4]. The transcription of the HPV genome is driven by two major promoters: in HPV type 16 (HPV16) genome, the early promoter P_{97} directs early gene transcription, while the late promoter P_{670} induces capsid expression. After initial unwinding of the replication origin by the coordinated action of the HPV E1 and E2 proteins, the HPV DNA replication progresses with the use of cellular replication proteins. For viral genome maintenance, the HPV genome is passively segregated by being tethered to host chromosomes, then passed into nuclei of daughter cells. Because of a lack of cell culture systems for efficient HPV propagation, molecular mechanisms of these processes are not fully understood.

Nucleolin is an abundant, ubiquitously expressed protein that is found in the nucleolus, the nucleoplasm, and on the cell surface, and is involved in regulation of ribosomal DNA (rDNA) transcription and the maturation of pre-ribosomal RNA [5]. In addition, nucleolin exerts several nuclear functions related to the transcription of several genes by the RNA polymerase II [6–8], genotoxic stress response [9], and chromosome congression in mitosis [10].

To gain new insights into how the dynamics of the HPV genome are regulated by host factors, we searched for cellular proteins that can bind to the two promoter regions of HPV16 using an unbiased proteomic approach. We describe the identification and characterization of nucleolin as an HPV16 genome-binding protein that may play a role in regulation of the HPV life cycle.

Materials and methods

Isolation of HPV16 genome-binding protein and its identification by peptide mass fingerprinting. Three HPV16 DNA fragments, I (nt 7791–120, 234 bp), II (nt 131–360, 230 bp), and III (nt 531–780, 250 bp), were generated by PCR using following primers: I forward, 5′biotin—TAC ATG AAC TGT GTA AAG GTT AGT CA-3′; I reverse, 5′-TGT GGG TCC TGA AAC ATT GCA GTT CTC TTT-3′; II forward, 5′biotin—AGA AAG TTA CCA CAG TTA TGC ACA GA-3′; II reverse, 5′-GTT CCA TAC AAA CTA TAA CAA TAA TGT CTA-3′; III forward, 5′biotin—CAA GAA CAC GTA GAG AAA CCC AGC TG-3′; III reverse, 5′-GTG TGT

* Corresponding author. Address: Pathogen Genomics Center, National Institute of Infectious Diseases, 4-7-1 Gakuen, Musashi-murayama, Tokyo 208-0011, Japan. Fax: +81 42 567 5632.
E-mail address: ikuki@nih.go.jp (I. Kukimoto).

0006-291X/$ - see front matter © 2009 Elsevier Inc. All rights reserved.
doi:10.1016/j.bbrc.2009.07.055

GCT TTG TAC GCA CAA CCG-3′. The biotinylated PCR products were purified using the Wizard SV gel and PCR clean-up system (Promega) and coupled to Dynabeads M-280 streptavidin (Dynal, Norway) in a buffer consisting of 10 mM Tris–HCl (pH 7.5), 0.5 mM EDTA, and 1 M NaCl. The HeLa nuclear extract was prepared by Dignam's procedure and incubated with the HPV16 DNA-coupled magnetic beads at 4 °C overnight. The beads were then washed three times in a wash buffer (10 mM Hepes, pH 7.9, 200 mM NaCl, 10 mM KCl, 1.5 mM $MgCl_2$, 1 mM DTT, 0.1% NP-40, and 10% glycerol). The bound proteins were released from the beads in SDS-sample buffer by boiling for 5 min and fractionated in a 4–20% gradient SDS–polyacrylamide gel (Daiichi Pure Chemicals, Japan), followed by silver staining. The 95-kDa protein band bound to fragment III was excised from the gel and subjected to in-gel trypsin digestion. The resultant peptide mixtures were analyzed by MALDI-QIT-TOF MS (AXIMA-QIT, Shimazu Biotech, Japan). Mascot software (Matrix Science) was used for protein identification.

Electrophoretic mobility shift assay (EMSA). The full-length cDNA of human nucleolin was amplified by RT-PCR from mRNA of HeLa cells. The resultant cDNA sequence completely matched the nucleolin sequence in the GenBank (NM 005381). To generate an expression plasmid for glutathione *S*-transferase (GST) fused nucleolin, the cDNA fragment encoding nucleolin amino acid (aa) from 289 to 710 was amplified by PCR with the full-length nucleolin cDNA as a template, and cloned into pGEX-2TK (GE Healthcare). GST–nucleolin and GST were expressed in *Escherichia coli* and purified using a GSTrap HT column and an AKTAprime (GE Healthcare). The EMSA was performed as described previously [11]. The DNA/protein complex was separated on a 5% polyacrylamide gel and visualized by autoradiography on X-ray films.

Chromatin immunoprecipitation (ChIP) assay. An expression plasmid for N-terminally FLAG-tagged nucleolin (FLAG-nucleolin) was constructed by cloning the full-length cDNA of nucleolin into p3xFLAG-CMV10 (Sigma). The ChIP assay was performed as described previously [11] with some modifications. Briefly, HeLa cells were transfected with pGL3-P_{670} or pGL3-Basic (Promega) together with the FLAG-nucleolin expression plasmid or p3xFLAG-CMV10 using FuGENE6 (Roche). At 48 h after the transfection, the cells were fixed with 1% formaldehyde at 37 °C for 5 min, lysed and sonicated using a Bioruptor (Cosmobio, Japan). The sonicated extract was immunoprecipitated with specific antibodies that had been coupled to Dynabeads M-280 sheep anti-mouse IgG (Dynal). Antibodies used were anti-FLAG M2 (Sigma), anti-nucleolin (MS-3, Santa Cruz, or 4E2, Abcam), or control mouse IgG (Santa Cruz). After washing the beads, the immunoprecipitated DNA/protein complexes were eluted, and reverse cross-linked. DNA was purified and subjected to PCR for HPV16 DNA (from nt 501 to 670), 18S rDNA, or pGL3-Basic. PCR primers were as follows: HPV16 forward, 5′-CCG GTC GAT GTA TGT CTT GTT GCA GAT CAT-3′; HPV16 reverse, 5′-CAT CCT CCT CCT CTG AGC TGT CAT TTA ATT-3′; 18S rDNA forward, 5′-GCC TGG ATA CCG CAG CTA GGA ATA ATG G-3′; 18S rDNA reverse, 5′-TTG ATT AAT GAA AAC ATT CTT GGC AAA TG-3′; pGL3-Basic forward, 5′-AGA CCC ACG CTC ACC GGC TCC AGA-3′; pGL3-Basic reverse, 5′-ACG AGC GTG ACA CCA CGA TGC CTG T-3′. The amounts of the immunoprecipitated DNA were quantified by real-time PCR analysis using a LightCycler 480 (Roche) with the LightCycler 480 SYBR Green I Master reagent (Roche). W12 cells were cultured in an undifferentiated state as described [12], and the ChIP assay was performed without plasmid transfection.

Generation of nucleolin-knockdown cells and Western blotting. The stable nucleolin-knockdown cell line derived from HeLa cells was established by transfection of an expression plasmid for small hairpin RNA (shRNA) against nucleolin and subsequent selection of cells in the presence of 10 μg/ml puromycin. The shRNA-expression plasmid was constructed by cloning the shRNA target sequence for nucleolin (5′-GGA AGA CGG TGA AAT TGA T-3′) [13] into pBAsi-hU6 (Takara, Japan). For Western blot analysis, cell extracts were prepared by boiling cells in SDS-sample buffer. Protein samples were separated on a 12% SDS–polyacrylamide gel, transferred to a nitrocellulose membrane (Schleicher & Schuell, Germany), and probed with a specified primary antibody and a peroxidase-conjugated secondary antibody. Antibodies used were anti-nucleolin (MS-3, Santa Cruz, or 3G4B20, Active Motif), anti-PCNA (PC10, Santa Cruz), and anti-FLAG M2. Specific proteins were visualized using an ECL Western blot detection system (GE Healthcare).

Results

Identification of nucleolin as a protein binding to an HPV16 genomic fragment

Two regions in the HPV16 genome were chosen as targets to screen for cellular proteins that might potentially regulate transcription and/or replication of HPV (I and III in Fig. 1A). Fragment I (nt 7791–120) contains the regulatory sequence for the HPV16 early promoter P_{97} and the replication origin, whereas fragment III (nt 531–780) includes the late promoter P_{670}. To find specific binding proteins for these fragments, fragment II (nt 131–360) was used as a control for comparison, because no particular binding proteins were assigned to this region. These DNA fragments were generated by PCR so as to have 5′-biotin-labeled ends, coupled to streptavidin-conjugated magnetic beads and then incubated in a nuclear extract prepared from HeLa cells. After washing the beads, bound proteins were released and separated by SDS–PAGE, followed by silver staining. Among many protein bands detected, fragment III selectively bound to a 95-kDa protein (Fig. 1B), while no specific proteins were detected for fragment I. To identify the 95-kDa protein, the band was excised from the gel, digested with trypsin, then subjected to peptide mass fingerprinting. The list of observed mass fingerprints significantly fitted the predicted mass fingerprint of human nucleolin (p value = 0.0094). Western blot analysis with an anti-nucleolin antibody verified an enrichment of nucleolin in the bound fraction of fragment III (Fig. 1C).

In vitro binding of nucleolin to the HPV16 DNA

An electrophoretic mobility shift assay (EMSA) revealed that a recombinant nucleolin bound to a site in the HPV16 genome from nt 591 to 620. Human nucleolin from amino acid 289 to 710, which contains four RNA-binding domains and a C-terminal glycine/arginine-rich region (Fig. 2A), was expressed as a fusion protein with GST (GST–nucleolin) in bacteria and affinity purified (Fig. 2B). This truncated nucleolin has been shown to exhibit DNA-binding activity [6]. GST–nucleolin was examined in EMSA for its capability to form a complex with overlapping DNA probes having the HPV16 sequences from nt 531 to 660. Among the HPV16 probes tested, probe f generated a shifted band with GST–nucleolin (Fig. 2C).

Nucleolin has been previously reported to bind to a different location in the HPV18 genome *in vitro*, and the binding site has been assigned to the sequence 5′-TTGCTTGCATAA-3′ (nt 7642–7653 in the HPV18 genome) [14]. Similarity between the HPV18 sequence and probe f was explored, and the same sequence motif, 5′-TTGCXXXCAXA-3′, was found in the two sequences (Fig. 2D, upper panel). To test whether this sequence motif was recognized by nucleolin, base substitutions that have been shown to abolish the nucleolin binding to the HPV18 site were introduced into probe f. The mutations completely disrupted the GST–nucleolin binding to the probe (Fig. 2D), demonstrating that nucleolin bound to this motif in probe f in a sequence-dependent manner.

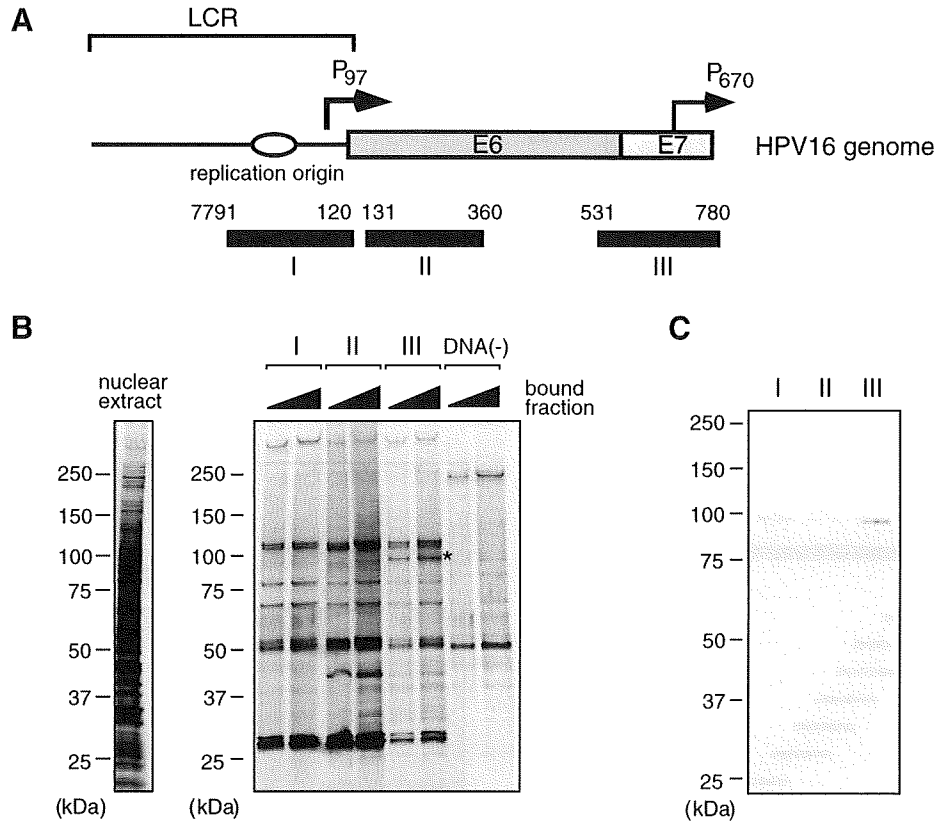

Fig. 1. Isolation of cellular proteins bound to HPV16 genomic fragments. (A) Schematic for locations of three HPV16 DNA fragments (I, II, and III) used to screen for binding proteins to HPV16 DNA. Numbers above the fragments indicate nucleotide positions in the HPV16 genome. The positions of the early promoter (P_{97}), the late promoter (P_{670}), the long control region (LCR), and the replication origin are presented. (B) The nuclear extract of HeLa cells was incubated with magnetic beads that were coupled with the HPV16 DNA fragments or with the beads alone. The bound fractions were recovered and resolved by SDS–PAGE, followed by silver staining. A 95-kDa band bound to fragment III is indicated by an asterisk. (C) Western blot analysis of the bound fractions using anti-nucleolin antibody (Santa Cruz).

GST–nucleolin bound to an HPV18 probe having the nucleolin-binding motif (Fig. 2D), which confirmed the integrity of our GST–nucleolin preparation. Additionally, several base substitutions were introduced into the motif in probe f (Fig. 2E, upper panel). All mutated probes gave rise to a band shift more efficiently than the original probe f (Fig. 2E), indicating that nucleolin recognizes this motif but it is not an optimal sequence for nucleolin binding.

Binding of nucleolin to the HPV16 DNA in cells

Chromatin immunoprecipitation (ChIP) analysis demonstrated that exogenous nucleolin bound to the HPV16 DNA in cells. An expression plasmid for FLAG-tagged nucleolin (FLAG-nucleolin) (Fig. 3A) was constructed and used for ChIP analysis. HeLa cells were transfected with the HPV16 reporter plasmid pGL3-P_{670}, which contains the HPV16 genomic region from nt 7003 to 868 [11], with or without the FLAG-nucleolin expression plasmid. In the presence of FLAG-nucleolin, an anti-FLAG antibody precipitated the HPV16 DNA fragment containing from nt 501 to 670 compared to the control IgG precipitate (Fig. 3B). Without FLAG-nucleolin expression, the anti-FLAG antibody did not precipitate the HPV16 DNA. The anti-FLAG antibody recovered an endogenous target of nucleolin, 18S rDNA, which indicated that exogenous FLAG-nucleolin behaved as endogenous one. The backbone plasmid lacking the HPV16 sequence was not precipitated with the anti-FLAG antibody in the presence of FLAG-nucleolin (Fig. 3C), demonstrating that the HPV16 sequence was responsible for the FLAG-nucleolin binding in cells. Similar results were obtained with human primary foreskin keratinocytes (data not shown), suggesting that the nucleolin binding to the HPV16 DNA is not specific to cancer cells.

Endogenous nucleolin also associated with the HPV16 DNA in cells. When the ChIP assay was performed in HeLa cells transfected with pGL3-P_{670} alone, the precipitate with an anti-nucleolin antibody showed an enrichment of the HPV16 DNA compared to basal level DNA obtained with a control antibody (Fig. 3D). To further examine binding properties of nucleolin to the HPV16 DNA in cells, a stable HeLa cell line expressing a reduced level of nucleolin was generated using an shRNA-mediated knockdown technique. Western blot analysis showed that the nucleolin level was reduced by one-third in the knockdown cells relative to parental cells (Fig. 3E). The ChIP assay revealed that the binding of nucleolin to the transfected HPV16 DNA was weakened in the knockdown cells compared to wild-type cells, and a similar reduction of nucleolin binding to rDNA loci was observed (Fig. 3F), suggesting that nucleolin's affinity for the HPV16 DNA is comparable to that for endogenous rDNA loci.

The ChIP assay was further extended to another human cell line, W12 cells, established from a cervical intraepithelial lesion and shown to maintain up to 1000 copies of the complete HPV16 genome as episomes in cell culture [12,15]. The immunoprecipitation with the anti-nucleolin antibody from the cross-linked chromatin of W12 cells enriched the HPV16 genomic DNA two to threefold compared to the control IgG precipitate, and a similar enrichment was observed with rDNA (Fig. 4). The results suggest that endogenous nucleolin is inherently bound to the HPV16 genome in the HPV16-infected cells.

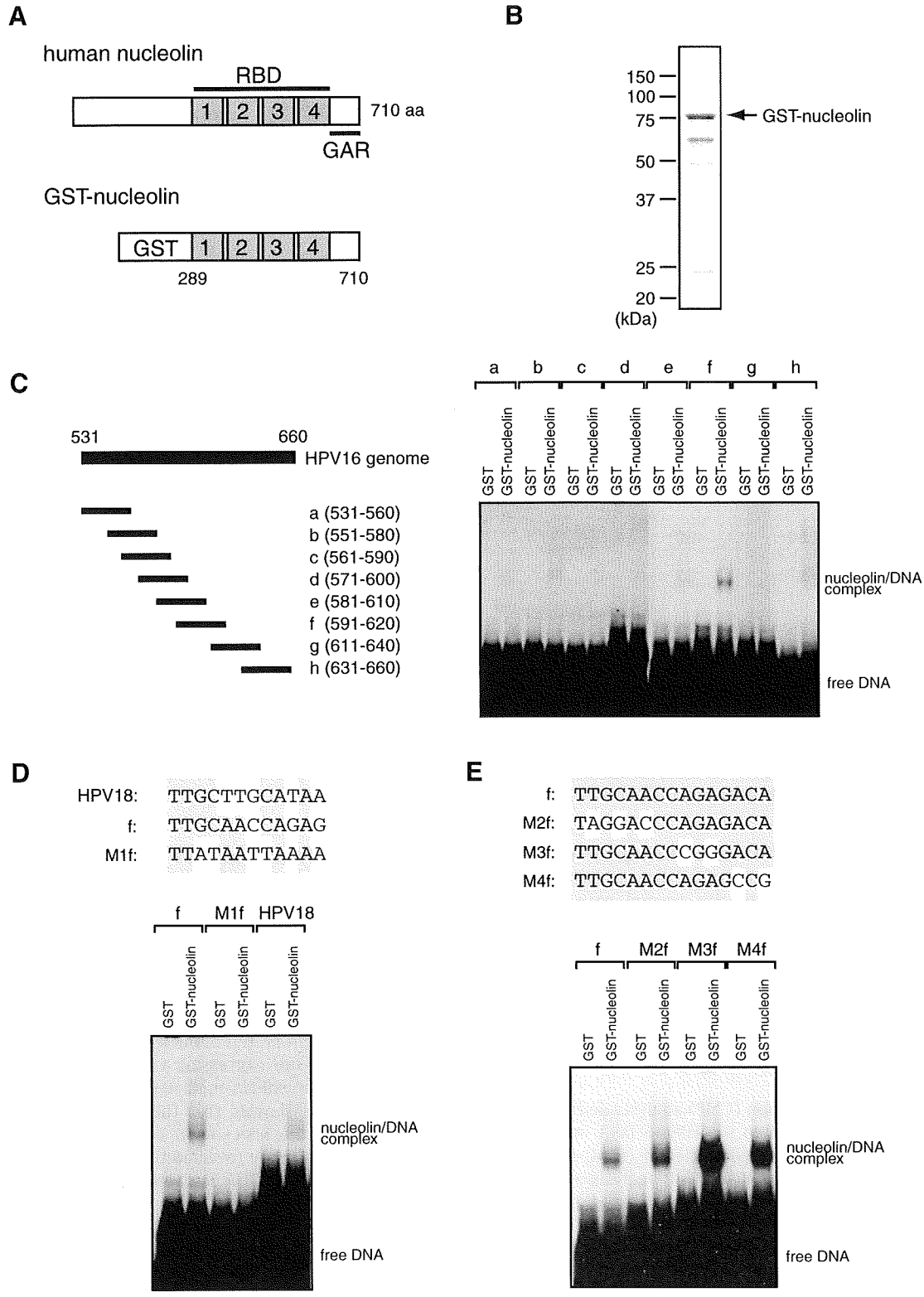

Fig. 2. *In vitro* binding of nucleolin to HPV16 DNA. (A) Schematic representation of human nucleolin and recombinant GST–nucleolin. Four RNA-binding domains (RBD1–4) and the glycine/arginine-rich region (GAR) are indicated. (B) SDS–PAGE analysis of GST–nucleolin with GelCode stain (Pierce). (C) EMSA showing a complex formation between GST–nucleolin and [^{32}P]-labeled oligonucleotide probes having the HPV16 genome sequence from nt 531 to 660. The genomic locations of the probes are presented on the left. (D) EMSA using mutated probe f to examine a sequence-specific binding of GST–nucleolin. Sequence alignment among the HPV18 nucleolin-binding sequence, probe f, and mutated probe f (M1f) is shown above. (E) Mutational analyses of probe f by EMSA. Base substitutions introduced into probe f are shown above.

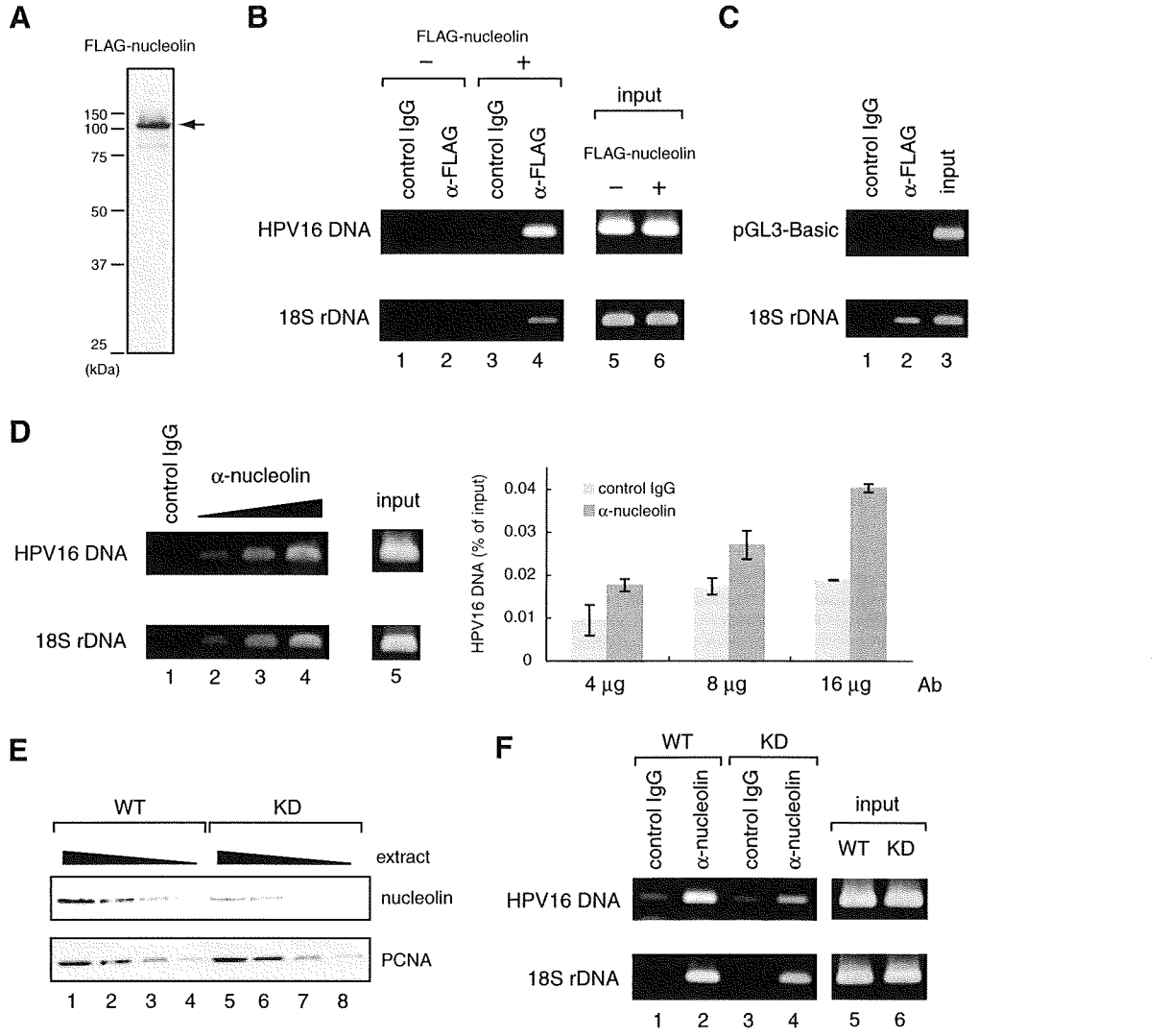

Fig. 3. Binding of nucleolin to HPV16 DNA in HeLa cells. (A) Western blot analysis of exogenous FLAG-nucleolin in HeLa cells using anti-FLAG antibody. (B) Chromatin immunoprecipitation analysis to detect binding of FLAG-nucleolin to HPV16 DNA in HeLa cells transfected with pGL3-P_{670}, which contains the HPV16 genome sequence from nt 7003 to 868, together with the FLAG-nucleolin expression plasmid or its backbone plasmid. Cross-linked FLAG-nucleolin/DNA complexes were immunoprecipitated with anti-FLAG antibody (lanes 2 and 4) or control mouse IgG (lanes 1 and 3), and the immunoprecipitated DNA was purified and subjected to PCR for the HPV16 DNA (nt 501–670) or 18S rDNA. The PCR products were analyzed by 1.5% agarose gel electrophoresis with ethidium bromide stain. Part (0.3%) of the input chromatin was analyzed. (C) ChIP analysis using HeLa cells transfected with pGL3-Basic and the FLAG-nucleolin expression plasmid. ChIP was performed with anti-FLAG antibody (lane 2) or control IgG (lane 1), followed by PCR for the pGL3-Basic sequence or 18S rDNA. (D) ChIP analysis to detect binding of endogenous nucleolin to the HPV16 DNA in HeLa cells transfected with pGL3-P_{670} alone. Anti-nucleolin antibody (Santa Cruz) was used to recover DNA/nucleolin complexes. The increasing amounts of antibodies (lanes 1 and 2, 4 μg; lane 3, 8 μg; lane 4, 16 μg) were used for ChIP. The amounts of immunoprecipitated HPV16 DNA were quantified by real-time PCR and shown as a percentage of the input HPV16 DNA in the right panel. Results are presented as means ± standard errors of two independent experiments. (E) Western blot analysis using total cell extracts from wild-type (WT) and nucleolin-knockdown (KD) HeLa cells. Twofold serially diluted extracts (lanes from 1 to 4 for WT cells; lanes from 5 to 8 for KD cells) were subjected to Western blotting with anti-nucleolin (Active Motif) or anti-PCNA antibodies. (F) ChIP analysis using wild-type and nucleolin-knockdown HeLa cells. Cross-linked nucleolin/DNA complexes from WT (lanes 1 and 2) and KD cells (lanes 3 and 4) were immunoprecipitated with anti-nucleolin antibody (Abcam) (lanes 2 and 4) or control mouse IgG (lanes 1 and 3), and the immunoprecipitated DNA was subjected to PCR for the HPV16 DNA (upper panel) or 18S rDNA (lower panel).

Discussion

Here we report the preferential binding of nucleolin to the HPV16 genomic region from nt 531 to 780. This genomic region is a "hot spot" for interactions with many cellular transcription factors that regulate the late promoter P_{670}. CCAAT displacement protein (CDP) and YY1 associate with this region to suppress the basal transcription from P_{670} [16–18], whereas multiple bindings of hSkn-1a and CCAAT/enhancer-binding protein β (C/EBPβ) to the same region relieved the repression by CDP and YY1, leading to activation of P_{670} [11,19]. Nucleolin bound to the HPV16 genomic region from nt 591 to 620 and recognized the sequence motif 5′-TTGCXXXCAXA-3′ from nt 604 to 614. This sequence partially overlaps with a binding site for C/EBPβ [11], which suggests functional competition between C/EBPβ and nucleolin for P_{670} regulation. However, contrary to the previous report showing an enhancing effect of nucleolin on the HPV18 early promoter [14], neither expression of FLAG-nucleolin nor knockdown of endogenous nucleolin by RNAi in HeLa cells had obvious effects on the P_{670} activity in a transient reporter assay (Sato et al., unpublished observation), questioning nucleolin's role in the HPV transcription.

Since nucleolin associated with the HPV16 genome in W12 cells, the nucleolin binding to the HPV16 genome likely occurs in the context of natural infection. With regard to maintenance of the viral genome, it is worth noting that a plasmid containing an HPV16 genomic fragment from the E6 to E7 region can be stably

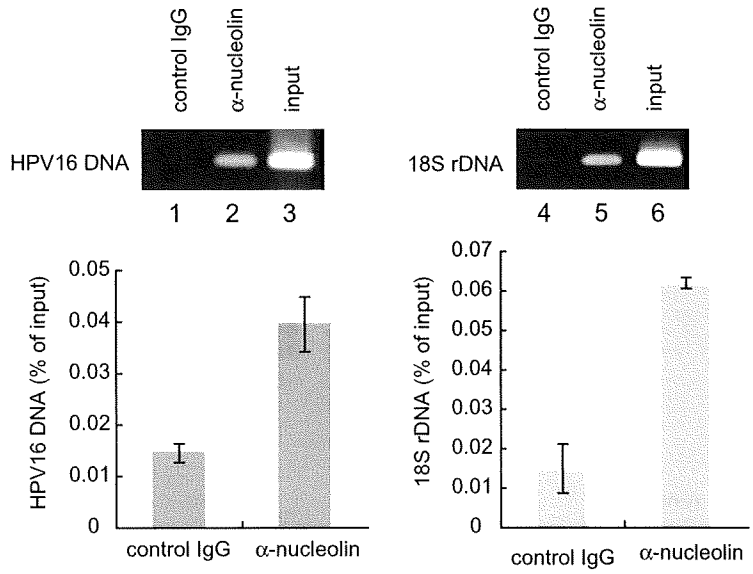

Fig. 4. Binding of nucleolin to HPV16 genome in W12 cells. ChIP analysis using W12 cervical neoplasia cells to detect binding of endogenous nucleolin to the HPV16 genome or rDNA. Cross-linked nucleolin/DNA complexes were immunoprecipitated with anti-nucleolin antibody (Abcam) (lanes 2 and 5) or control mouse IgG (lanes 1 and 4), and the immunoprecipitated DNA was subjected to PCR for the HPV16 DNA (nt 501–670) (lanes 1 and 2) or 18S rDNA (lanes 4 and 5). Part (0.3%) of the input chromatin was analyzed (lanes 3 and 6). The amounts of immunoprecipitated DNA were quantified by real-time PCR and shown as a percentage of the input DNA. Results are presented as means ± standard errors of two independent experiments.

maintained in human cells in the absence of the viral E1 and E2 proteins [20]. This finding indicates a genome maintenance mode that is completely dependent on host proteins (independent of virally encoded proteins). Given that the nucleolin-binding site located from nt 604 to 614 lies in the E7 region, nucleolin may facilitate E1/E2-independent maintenance of the HPV genome. Detailed analysis of subcellular localization of nucleolin has demonstrated that nucleolin becomes localized at the chromosome periphery during mitosis in HeLa cells [10]. Thus, nucleolin might be involved in tethering the HPV genome to host chromosomes, which prevents the HPV genome from diffusing into cytoplasm during mitosis.

Lastly, nucleolin has been reported to play roles in the life cycle of other human viruses. Nucleolin interacts with nonstructural protein 5B of hepatitis C virus (HCV) and this interaction seems to be required for efficient replication of HCV [13]. Nucleolin localizes to the viral replication compartments of herpes simplex virus type 1 (HSV-1) in the nucleus during productive infection and the knockdown of nucleolin by RNAi inhibits HSV-1 replication [21]. Thus, it will be of particular interest to investigate the exact function of nucleolin in the HPV life cycle in future studies.

Acknowledgment

We thank Dr. Paul Lambert for providing us with the W12 cell line.

References

[1] H. zur Hausen, Papillomavirus infections—a major cause of human cancers, Biochim. Biophys. Acta 1288 (1996) F55–F78.
[2] M.S. Longworth, L.A. Laimins, Pathogenesis of human papillomaviruses in differentiating epithelia, Microbiol. Mol. Biol. Rev. 68 (2004) 362–372.
[3] F. Thierry, Transcriptional regulation of the papillomavirus oncogenes by cellular and viral transcription factors in cervical carcinoma, Virology 384 (2009) 375–379.
[4] A.A. McBride, Replication and partitioning of papillomavirus genomes, Adv. Virus Res. 72 (2008) 155–205.
[5] F. Mongelard, P. Bouvet, Nucleolin: a multiFACeTed protein, Trends Cell Biol. 17 (2007) 80–86.
[6] E. Grinstein, Y. Du, S. Santourlidis, J. Christ, M. Uhrberg, P. Wernet, Nucleolin regulates gene expression in CD34-positive hematopoietic cells, J. Biol. Chem. 282 (2007) 12439–12449.
[7] S. Samuel, J.C. Twizere, K.K. Beifuss, L.R. Bernstein, Nucleolin binds specifically to an AP-1 DNA sequence and represses AP1-dependent transactivation of the matrix metalloproteinase-13 gene, Mol. Carcinog. 47 (2008) 34–46.
[8] G.G. Ying, P. Proost, J. van Damme, M. Bruschi, M. Introna, J. Golay, Nucleolin, a novel partner for the Myb transcription factor family that regulates their activity, J. Biol. Chem. 275 (2000) 4152–4158.
[9] K. Kim, D.D. Dimitrova, K.M. Carta, A. Saxena, M. Daras, J.A. Borowiec, Novel checkpoint response to genotoxic stress mediated by nucleolin-replication protein a complex formation, Mol. Cell. Biol. 25 (2005) 2463–2474.
[10] N. Ma, S. Matsunaga, H. Takata, R. Ono-Maniwa, S. Uchiyama, K. Fukui, Nucleolin functions in nucleolus formation and chromosome congression, J. Cell Sci. 120 (2007) 2091–2105.
[11] I. Kukimoto, T. Takeuchi, T. Kanda, CCAAT/enhancer binding protein beta binds to and activates the P670 promoter of human papillomavirus type 16, Virology 346 (2006) 98–107.
[12] S. Jeon, B.L. Allen-Hoffmann, P.F. Lambert, Integration of human papillomavirus type 16 into the human genome correlates with a selective growth advantage of cells, J. Virol. 69 (1995) 2989–2997.
[13] T. Shimakami, M. Honda, T. Kusakawa, T. Murata, K. Shimotohno, S. Kaneko, S. Murakami, Effect of hepatitis C virus (HCV) NS5B-nucleolin interaction on HCV replication with HCV subgenomic replicon, J. Virol. 80 (2006) 3332–3340.
[14] E. Grinstein, P. Wernet, P.J. Snijders, F. Rosl, I. Weinert, W. Jia, R. Kraft, C. Schewe, M. Schwabe, S. Hauptmann, M. Dietel, C.J. Meijer, H.D. Royer, Nucleolin as activator of human papillomavirus type 18 oncogene transcription in cervical cancer, J. Exp. Med. 196 (2002) 1067–1078.
[15] M.A. Stanley, H.M. Browne, M. Appleby, A.C. Minson, Properties of a non-tumorigenic human cervical keratinocyte cell line, Int. J. Cancer 43 (1989) 672–676.
[16] W. Ai, E. Toussaint, A. Roman, CCAAT displacement protein binds to and negatively regulates human papillomavirus type 6 E6, E7, and E1 promoters, J. Virol. 73 (1999) 4220–4229.
[17] W. Ai, J. Narahari, A. Roman, Yin yang 1 negatively regulates the differentiation-specific E1 promoter of human papillomavirus type 6, J. Virol. 74 (2000) 5198–5205.
[18] K. Sato, T. Takeuchi, I. Kukimoto, S. Mori, T. Yasugi, T. Yano, Y. Taketani, T. Kanda, Human papillomavirus type 16 P670 promoter is negatively regulated by CCAAT displacement protein, Virus Genes 35 (2007) 473–481.
[19] I. Kukimoto, T. Kanda, Displacement of YY1 by differentiation-specific transcription factor hSkn-1a activates the P(670) promoter of human papillomavirus type 16, J. Virol. 75 (2001) 9302–9311.
[20] D. Pittayakhajonwut, P.C. Angeletti, Analysis of cis-elements that facilitate extrachromosomal persistence of human papillomavirus genomes, Virology 374 (2008) 304–314.
[21] A. Calle, I. Ugrinova, A.L. Epstein, P. Bouvet, J.J. Diaz, A. Greco, Nucleolin is required for an efficient herpes simplex virus type 1 infection, J. Virol. 82 (2008) 4762–4773.

Eur J Pediatr (2009) 168:347–349
DOI 10.1007/s00431-008-0744-8

SHORT REPORT

Neonatal pertussis presenting as acute bronchiolitis: direct detection of the *Bordetella pertussis* genome using loop-mediated isothermal amplification

Akari Nakamura · Takashi Sakano · Tetsuo Nakayama · Hiroko Shimoda · Yasuyuki Okada · Ryuzo Hanayama · Katsuhiro Nomoto · Tetsushi Suto · Yoshihisa Kinoshita · Takeki Furue · Hiroaki Ono · Toshiyuki Ohta

Received: 19 January 2008 / Accepted: 14 April 2008 / Published online: 6 June 2008

Abstract We report a 28-day-old female infant with pertussis presenting as severe acute bronchiolitis with cyanosis. On admission, the patient's symptoms were similar to those of acute bronchiolitis. However, occasional apneic episodes with cyanosis and peripheral lymphocytosis suggested neonatal pertussis and prompted us to examine the presence of *Bordetella pertussis* using loop-mediated isothermal amplification (LAMP) based on the insertion sequence IS481. LAMP of the nasopharyngeal and intratracheal aspirates was positive for *B. pertussis* and a diagnosis of neonatal pertussis was made. As the clinical features of pertussis in neonates and early infancy are not characteristic, LAMP is a useful tool for rapid diagnosis of *B. pertussis* infection.

A. Nakamura · H. Shimoda · Y. Okada · R. Hanayama · K. Nomoto
Department of Pediatrics, National Hospital Organization, Higashi-Hiroshima Medical Center, Higashi-Hiroshima, Japan

T. Sakano (✉) · T. Suto · Y. Kinoshita · T. Furue · H. Ono · T. Ohta
Department of Pediatrics, Hiroshima Prefectural Hospital, 1-5-54, Ujinakanda Minamiku, Hiroshima, Japan
e-mail: t-sakano@hph.pref.hiroshima.jp

T. Nakayama
Laboratory of Viral Infection I, Kitasato Institute for Life Sciences, Tokyo, Japan

A. Nakamura
Jike 513, Saijo-cho, Higashi-Hiroshima, Hiroshima 739–0041, Japan
e-mail: nakamura_akari@hiro-hosp.jp

Keywords *B. pertussis* · Bronchiolitis · LAMP · Neonatal pertussis

Abbreviations
LAMP Loop-mediated isothermal amplification

Case report

A 28-day-old female infant, who was born at 39 weeks gestation weighing 2,928 g, was referred to us because of cough, wheezing, and cyanosis. The infant had begun to have manifestations of mild viral upper respiratory tract infection at the age of 21 days. The respiratory symptoms worsened abruptly and cyanosis was observed on the day before admission. The child's mother and 6-year-old sister, who had both received DPT vaccination, had complained of mild coughs two weeks before the onset of the patient's illness, but had not been treated with any antibiotics.

On admission to our hospital, the patient was dyspneic without pyrexia, and oxygen saturation decreased to 88% during a fit of coughing. The heart rate was 160/min and the respiratory rate was 45–60/min. Routine hematological tests showed a white blood cell count of 28,600/μl with a lymphocyte count of 16,331/μl, and C-reactive protein was 0.04 mg/dl. Chest X-ray showed mild pulmonary emphysema. The nasopharyngeal fluid was negative on immunoassays for respiratory syncytial virus, influenza A and B, and adenovirus. The patient's symptoms on admission strongly suggested bronchiolitis. In addition, the apneic episodes with cyanosis and lymphocytosis suggested

neonatal pertussis. Initially, the patient was treated with piperacillin and hydrocortisone. However, her condition deteriorated and she developed severe apnea and bradycardia during the night after admission. Chest X-ray indicated the presence of atelectasis in the upper lobe of the right lung. Following increasing respiratory distress over the next two days, intubation was required, and she was ventilated at high pressure. Clarithromycin was started on day three after admission. Despite undergoing mechanical ventilation, the patient had frequent episodes of severe apnea with bradycardia and required manual ventilation for recovery. Nasopharyngeal and intratracheal aspirates obtained on day five were positive for *Bordetella pertussis* using a loop-mediated isothermal amplification (LAMP) assay based on the insertion sequence IS481 target (Fig. 1). PCR analyses of the nasopharyngeal and intratracheal aspirates were also positive for *B. pertussis* (data not shown). Viral isolation and bacterial cultures from intratracheal aspirates were negative. The patient made favourable progress from the fifth day of intubation and ventilation was stopped on the eighth day. Piperacillin and clarithromycin were continued for eight days and three weeks, respectively. LAMP remained positive 30 days after initiation of treatment, when the infant had no clinical manifestations of pertussis, and was finally negative for the presence of the *B. pertussis* genome on the 33rd day. LAMP was negative for *B. pertussis* in the patient's parents and sister.

Discussion

Young infants with *B. pertussis* infection present with atypical symptoms, including apnea, cyanosis, and wheezing, and the laboratory findings, like leukocytosis and lymphocytosis, are not always specific. Therefore, such cases are often treated as acute bronchitis or bronchiolitis. The initial manifestations found in our patient strongly suggested that she had contracted acute bronchiolitis. Manifestations such as bronchiolitis are not rare in early infantile pertussis, and Sotomayor et al. reported that a diagnosis of bronchiolitis or pneumonia was made in 14 of 46 infantile pertussis cases in the early stages [4]. Although pertussis can be diagnosed from culture and serological studies, culture requires 7–10 days to isolate *B. pertussis* and serology is frequently negative in young infants with pertussis, like our patient. Confirmation of the diagnosis by serology requires acute- and convalescent-phase sera, delaying the diagnosis of *B. pertussis* infection.

PCR is more sensitive than culture-based methods and is not readily affected by prior antibiotic therapy. Its main disadvantage is that PCR assays have limited availability, and false positives can occasionally occur [3]. In our case, *B. pertussis* was detected using both LAMP and PCR. LAMP has been developed as a novel method to amplify DNA, and it has been reported to be a rapid method for the diagnosis of *B. pertussis* infection that requires only about 60 min and is less expensive than PCR [2]. The sensitivity and specificity of LAMP for *B. pertussis* are 83 and 95%, respectively [2]. The LAMP assay promises to become a useful tool for the rapid diagnosis of pertussis in clinical laboratories without requiring specific equipment, such as a thermal cycler and electrophoresis system. As cross-reactivity with *B. bronchiseptica* in IS481-based PCR has been reported, the possibility that a LAMP assay based on an IS481 target might also cross-react with *B. bronchiseptica* cannot be excluded completely [2]. However, with few exceptions, *B. bronchiseptica* is not pathogenic in humans, and our patient had certainly contracted *B. pertussis* infection.

Of particular interest is the persistence of a positive LAMP reaction long after commencing treatment. Bonacorsi et al. reported a very-low-birth-weight neonate in whom treatment with josamycin was unsuccessful and PCR for *B. pertussis* was positive for 78 days after the initial treatment [1]. The reason for the persistence of positive DNA results remains unclear, but the high sensitivity of LAMP and the difficulty of eliminating pathogens in infants with compromised immunity may contribute to long-term persistence of the *B. pertussis* genome. Further studies of culture- and genome-based methods for the detection of *B. pertussis* are required to clarify the optimal duration of treatment for neonatal *B. pertussis* infection.

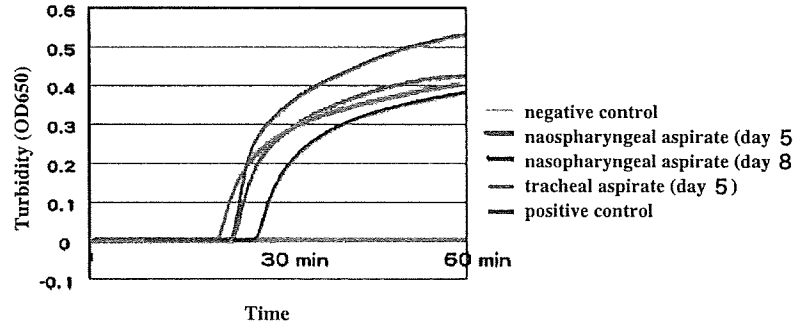

Fig. 1 The results of LAMP for detecting the *Bordetella pertussis* genome. LAMP of nasopharyngeal (on days 5 and 8) and tracheal (on day 5) aspirates showed a positive reaction within 30 min

References

1. Bonacorsi S, Farnoux C, Biget P, Caro V, Aizenfisz S, Benhayoun M, Aujard Y, Guiso N, Bingen E (2006) Treatment failure of nosocomial pertussis infection in a very-low-birth-weight neonate. J Clin Microbiol 44(10):3830–3832
2. Kamachi K, Toyoizuumi-Ajisaka H, Toda K, Soeung SC, Sarath S, Nareth Y, Horiuchi Y, Kojima K, Takahashi M, Arakawa Y (2006) Development and evaluation of a loop-mediated isothermal amplification method for rapid diagnosis of *Bordetella pertussis* infection. J Clin Microbiol 44(5):1899–1902
3. Senanayake S (2007) Pertussis in Australia today. A disease of adolescents and adults that can kill infants. Aust Fam Physician 36 (1–2):51–56
4. Sotomayor J, Weiner LB, McMillan JA (1985) Inaccurate diagnosis in infants with pertussis. An eight-year experience. Am J Dis Child 139:724–727

Vaccine 27 (2009) 234–242

Contents lists available at ScienceDirect

Vaccine

journal homepage: www.elsevier.com/locate/vaccine

Histidine at position 1042 of the p150 region of a KRT live attenuated rubella vaccine strain is responsible for the temperature sensitivity

Masafumi Sakata[a], Katsuhiro Komase[b], Tetsuo Nakayama[a,*]

[a] Laboratory of Viral Infection I, Kitasato Institute for Life Sciences, 5-9-1 Shirokane, Minato-ku, 108-8641 Tokyo, Japan
[b] Department of Virology III, National Institute of Infectious Diseases, Tokyo, Japan

ARTICLE INFO

Article history:
Received 9 July 2008
Received in revised form 2 October 2008
Accepted 19 October 2008
Available online 7 November 2008

Keywords:
Rubella virus
KRT vaccine strain
Temperature sensitivity
Reverse genetics

ABSTRACT

The Japanese live attenuated KRT rubella vaccine strain has a temperature sensitivity (*ts*) phenotype. The objective of this study is to identify the region responsible for this phenotype. Genomic sequences of the KRT strain and the wild-type strain (RVi/Matsue.JPN/68) with the non-*ts* phenotype were investigated and reverse genetic systems (RG) for these strains were developed. The *ts* phenotype of KRT varied drastically on replacement of the p150 gene (encoding a methyltransferase and a nonstructural protease). Analysis of four chimeric viruses showed the region responsible for the *ts* phenotype to be located between Bsm I and Nhe I sites (genome position 2803–3243). There were two amino acid differences at positions 1007 and 1042. Mutations were introduced into the KRT cDNA clone, designated G1007D, H1042Y and G1007D-H1042Y. H1042Y and G1007D-H1042Y grew well at a restrictive temperature with a 100-fold higher titer than G1007D and the KRT strain, but a 10-fold lower titer than RVi/Matsue.JPN/68. Since the growth of H1042Y was not completely the same as that of the wild-type strain at the restrictive temperature, we also assessed whether other genomic regions have an additive effect with H1042Y on the *ts* phenotype. H1042Y-RViM SP having structural proteins of RVi/Matsue.JPN/68 grew better than H1042Y, similar to RVi/Matsue.JPN/68. Thus, we concluded that one mutation, of the histidine at position 1042 of p150, was essential for the *ts* phenotype of the KRT strain, and structural proteins of KRT had an additive effect with H1042Y on the *ts* phenotype.

1. Introduction

Rubella virus (RV) is the sole member of the genus *Rubivirus* in the family *Togaviridae*. RV is an enveloped, single-stranded, positive-sense RNA virus with an approximately 10-kb genome, having a cap structure at the 5′ end of the genome and polyA tail at the 3′ end. The genome contains three untranslated regions (UTRs) and two open reading frames (ORFs). One UTR is located at the 5′ end, one at the 3′ end, and one between the ORFs. The UTR between the two ORFs is the junction-UTR (J-UTR). The 5′ end ORF encodes two nonstructural proteins (NSPs) named p150 and p90, while the 3′ end ORF encodes three structural proteins (SPs); capsid protein and the two envelope proteins, E1 and E2. NSPs are translated from genomic RNA and act as a viral genome replication complex. The full-length negative-sense RNA (cRNA) is replicated from genomic RNA. cRNA acts as a template for replicating progeny viral RNA and sub-genomic RNA (SG RNA). Three SPs, capsid, E2, and E1, are translated from SG RNA to form virion structures. Nucleocapsids are comprised of the genomic RNA and capsid protein, and constitute progeny virions surrounded by a lipid viral membrane embedded with E1 and E2 [1,2].

RV infection is one of many transmissible diseases in infants and children. Most patients with RV demonstrate mild symptoms, maculopapular rash, lymphadenopathy, low-grade fever, conjunctivitis, sore throat and arthralgia, and recover in several days without any complications or sequelae. However, infection in unimmunized women during the early stages of pregnancy, especially within the first trimester, cause fetal death or congenital rubella syndrome (CRS). CRS is characterized by multiple malformations: deafness, cataracts, cardiac disease and neurological abnormalities [3–5]. For the prevention of CRS, live attenuated vaccines have been used in vaccination programs in many countries. Recently, in the United States and several European countries, the indigenous circulation of rubella virus has been disrupted and CRS has been eliminated [3]. The prevention of CRS and rubella epidemics mainly depends on efficacious vaccination programs. In Japan, a nationwide outbreak of rubella has not occurred since 1993, but some cases of CRS in sporadic regional outbreaks have been reported. Rubella infection still remains an important issue in Japan and the accelerated control of RV infection is anticipated for the elimination of CRS.

* Corresponding author.
E-mail address: tetsuo-n@lisci.kitasato-u.ac.jp (T. Nakayama).

0264-410X/$ – see front matter © 2008 Elsevier Ltd. All rights reserved.
doi:10.1016/j.vaccine.2008.10.049

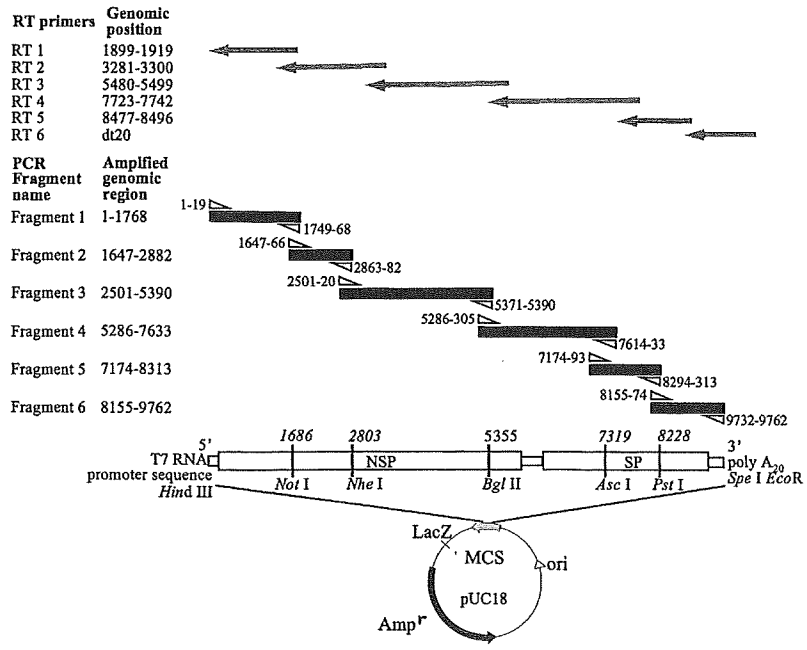

Fig. 1. Construction of the infectious cDNA clones from KRT and RVi/Matsue.JPN/68. Gray arrows indicate the RT primers and direction of cDNA synthesis, and numbers are genomic positions of RT primers. The six RT products were amplified by PCR with primer sets. Open arrowheads indicate the positions of primers. Six PCR fragments were cloned at Eco RI and Hind III in the MCS of pUC18. The full-length cDNA clones were constructed by combining each cDNA clone, using the restriction enzyme sites described in the panel.

Four live attenuated rubella vaccine strains have been used in Japan. The attenuation process differed for each strain with serial passages of the wild-type rubella viruses in different primary cells and cell lines at 35 °C or less [6]. Ohtawara et al. [7] also reported that all Japanese rubella vaccine strains exhibit unique characteristics of temperature sensitivity (*ts*) in cultured cells. Although the wild-type strains show approximately 10-fold lower infective titers at a restrictive temperature of 39 °C than at a permissive temperature of 35 or 37 °C, the vaccine strains with *ts* phenotype demonstrate growth at 39 °C that is 1/1000 that at 35 or 37 °C.

In this study, we determined the complete genomic sequences of both the KRT live attenuated rubella vaccine and the wild-type RVi/Matsue.JPN/68 strain circulating at the same time and in the same region as the progenitor wild-type of KRT. Reverse genetic systems (RG) for the two strains were developed [8–13], and a series of recombinant chimeric viruses and point-mutated viruses were generated from KRT and RVi/Matsue.JPN/68 and point-mutated viruses were generated to investigate the region responsible for the *ts* phenotype. Through infection experiments in cultured cells, the p150 gene, especially the histidine at position 1042, was determined to be responsible for the *ts* phenotype of the KRT strain. This is the first report to identify the region responsible for the *ts* phenotype of a live attenuated rubella vaccine at the molecular level.

2. Materials and methods

2.1. Cells and viruses

Vero and RK13 cells were maintained in Eagle's minimum essential medium (MEM) (Sigma–Aldrich, MO, USA) supplemented with 5% fetal bovine serum (FBS), penicillin (100 U/ml) and streptomycin (100 U/ml). RVs of the KRT and RVi/Matsue.JPN/68 strains propagated in RK13 and Vero cells were used in this study. The KRT vaccine strain was supplied by the Kitasato Institute Research Center Biologicals and the wild-type RVi/Matsue.JPN/68 strain was kindly provided by Y. Umino, NIID Japan.

2.2. Preparation of viral RNA, amplification of viral cDNA and nucleotide sequencing

Monolayers of RK13 cells grown in 6-well plates were infected with RVi/Matsue.JPN/68, and the culture medium was harvested on day 5 post-infection. Viral RNA was extracted from the culture medium of RVi/Matsue.JPN/68 and bulk material of the KRT vaccine with MagExtractor -Viral RNA- (TOYOBO, Osaka, Japan) following the instruction manual, and used for first-strand cDNA synthesis. The primers used for reverse transcription (RT) and the polymerase chain reaction (PCR) are shown in Fig. 1. First-strand cDNA synthesis was carried out at 50 °C for 1 h in a 10-μl reaction mixture containing viral RNA, 5 pmol of reverse primer based on the RV genome or poly deoxythymidine (poly dT) primer, 100 U of SuperScript III reverse transcriptase (Invitrogen, CA), 40 U of RNasin Plus Ribonuclease Inhibitor (Promega, Madison, WI) 5.0 mM DTT, 125 μM dNTP Mix (125 μM each of dATP, dGTP, dCTP and dTTP), 50 mM Tris–HCl, 75 mM KCl, and 300 μM $MgCl_2$. First-strand cDNA, PCR, and sequencing primers were designed by referring to the sequence reports of TO-336 wt (Genbank accession number AB047330), TO-336vac (AB047329) and RA27/3 vaccine (L78917). For sequencing the 5′ and 3′ end of the genome, 5′ and 3′-Full RACE core kits (TakaRa, Shiga, Japan) were used with 5′-TCACTGACCTGCATCT-3′ (genome position [gp] 219–234) and poly dT. The first-strand cDNA was amplified by nested or semi-nested PCR in six overlapping fragments. The amplification was performed in a 50-μl reaction mixture, containing cDNA, 25 pmol of the primer set, 5% dimethyl sulfoxide (DMSO) and *TaKaRa La Taq* polymerase (TaKaRa) with the PCR mixture provided by the manufacturer. The reaction was carried out under thermal cycling conditions for 3 min at 95 °C followed by 30 cycles of 20 s at 95 °C, 30 s at 62 °C, and 90 s at 68 °C with some modifications. PCR products were excised and used for sequencing with a DYEnamic ET Terminator Cycle sequencing Kit (GE Healthcare Bio-Science, NJ), and analyzed with a 377 XL DNA sequencer (Applied Biosystems, CA). M13RV and M13m4 sequencing primers were used to determine the nucleotide sequence of the

Table 1
Comparison of nucleotide (nt) and amino acid (a.a.) sequences between KRT (vac) and RVi/Matsue.JPN/68 (wt).

		NSP[b]			SP[c]			
	5′UTR[a]	p150	p90	J-UTR[a]	C	E2	E1	3′UTR[a]
nt	40	3903	2442	123	900	846	1443	62
vac/wt[d] (%)	2 (5.0)	69 (1.77)	65 (2.66)	5 (4.17)	27 (3.0)	27 (3.19)	36 (2.49)	1 (1.61)
a.a.		1301	814		300	282	481	
vac/wt[d]		15	1		4	8	5	
(%)		(1.15)	(0.12)		(1.33)	(2.84)	(1.04)	

[a] UTR was an untranslated region.
[b] NSP was a nonstructrual precursor polyprotein encoding two nonstructural proteins, p150 and p90.
[c] SP was a structural precursor polyprotein encoding three proteins, capsid, E2, and E1.
[d] The number of nucleotides or amino acid residues differed between the KRT vaccine (vac) and wild RVi/Matsue.JPN/68 (wt) strains.

5′ and 3′ ends of the genome cloned into the multi-cloning site (MCS) of pUC18 that were constructed with the 5′ and 3′-Full RACE core kits.

2.3. Construction of infectious cDNA clones of KRT and RVi/Matsue.JPN/68

Based on the entire genome sequence of the KRT and RVi/Matsue.JPN/68 strains, viral cDNA was synthesized with six primers and cDNAs were amplified with KOD plus DNA polymerase (TOYOBO). The amplified regions and primer sets are summarized in Fig. 1. For cloning of the cDNAs into the MCS of pUC18, Hind III (*italic: aagctt*) and Eco RI (*italic: gaattc*) restriction enzyme sequences were linked to the 5′ end of the forward and reverse primers, respectively. These fragments were digested with Hind III and Eco RI and cloned into the MCS of pUC18. All fragments inserted into the plasmid were confirmed by using appropriate restriction enzymes and sequenced. Individual clones were digested with restriction enzymes as shown in Fig. 1 and ligated with each other to construct the full-length cDNA clones of KRT and RVi/Matsue.JPN/68. The T7 RNA promoter sequence was introduced at the 5′ end and a polyA tail at the 3′ end of the full-length cDNA, and sub-cloning of cDNAs covering the 5′ and 3′ ends of the viral genome was carried out. The T7 RNA promoter sequence (double underline) was introduced after amplification, using as a forward primer 5′-tgtc*aagctt*taatacgactcactataggCAATGGGAGCTATCGGACC-3′ for KRT and 5′-tgtc*aagctt*taatacgactcactataggCAATGGAAGCTATCGGACC-3′ for RVi/Matsue.JPN/68 (gp 1–19) with the reverse primer 5′-agtc*gaattc*ACTCGGCAGCAGACCAGCCG-3′ (gp 2863–2882). A polyA tail was also introduced after the amplification, using as a forward primer, 5′-agta*aagctt*GTCTCTTGATCACGCCCTCG-3′ (gp 8110–8129) and reverse primer, 5′-atta*gaattcactagt*T_{19}CTATGCAGCAACAG-3′ (gp 9649–9762), which includes restriction sites for Eco RI and Spe I (*italic: actagt*) downstream of the poly dT_{19} tract [11]. Modified 5′ and 3′ ends were confirmed by sequencing and reintroduced into the full-length cDNA with appropriate restriction enzymes. The infectious cDNA clones constructed from KRT and RVi/Matsue.JPN/68 were named pKRT and pRViM, respectively.

2.4. Construction of cDNA clones of recombinant chimeric viruses and point mutation viruses

Recombinant cDNA clones based on pKRT and pRViM were generated by using appropriate restriction enzymes. Along with the genome structure of RV, we generated eight recombinant infectious cDNA clones designated pKRT-rec1–8. The recombinant construct pKRT-rec1 was generated by replacing the region from Hind III to Nco I (gp 5′ end to 39) containing the 5′ UTR sequence, respectively. The recombinant rec2 and rec3 constructs which cover the entire ORF of the NSP genes (p150 and p90) were generated by replacing the region between the two Nco I sites (gp 39–4023) containing most of the p150 gene and the region from Bsm I to Not I (gp 3243–6623) containing most of the p90 gene, respectively. The recombinant rec4 construct was generated by replacing the region between the two PspX I sites (gp 6338–6557) containing the J-UTR sequence. As for the ORF of the SP genes, the recombinant rec5, rec6, and rec7 constructs were generated by replacing the region from Xmn I to Asc I (gp 6514–7319), Asc I to Pst I (gp 7319–8232), and Pst I to AsiS I (gp 8232–9457), for C, E2, and E1, respectively. The recombinant rec8 construct was generated by replacing the region from AsiS I to Eco RI (gp 9457–3′ end) containing the 3′ UTR sequence. To construct the recombinant cDNA clones in the p150 region, we generated the four recombinant constructs pKRT-p150 rec1, 2, 3, and 4 by using the restriction enzyme sites Mfe I (gp 126),

Table 2
Differences in amino acid residues of KRT and RVi/Matsue.JPN/68.

Coding region	Amino acid position	Strain	
		KRT	RVi/Matsue.JPN/68
p150	295	A	T
	407	S	G
	466	L	F
	483	A	T
	674	V	I
	717	L	S
	739	P	H
	740	S	L
	751	V	A
	777	E	G
	790	V	A
	795	G	D
	961	V	A
	1007	G	D
	1042	H	Y
p90	195	I	T
Capsid	11	G	A
	34	P	S
	72	K	R
	226	H	T
E2	6	V	A
	7	H	D
	14	P	L
	104	S	P
	105	L	F
	122	S	A
	234	P	S
	235	P	S
E1	5	A	T
	177	D	N
	203	M	L
	333	T	A
	398	R	A

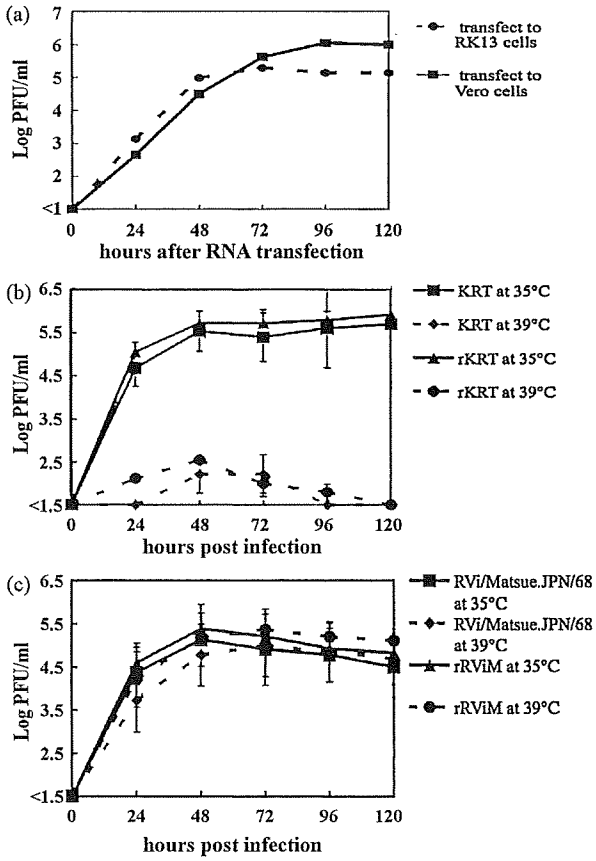

Fig. 2. Recovery of the clone virus from an infectious cDNA clone of pKRT and the growth properties of the clone and original virus. (a) Recovery of infectious clone. Vero and RK13 cells were transfected with viral genomic RNA synthesized from pKRT. The culture medium was harvested and the infective titer was determined by the plaque assay. The average titer for two independent experiments is shown. (b) Growth kinetics of KRT and rKRT at 35 and 39 °C. RK13 cells were infected at a MOI of 0.01. The culture medium was harvested and the infective titer was measured by the plaque assay. The results show the average for three independent experiments and the error bar indicates ±standard deviation (SD). (c) Growth kinetics of RVi/Matsue.JPN/68 and rRViM at 35 and 39 °C.

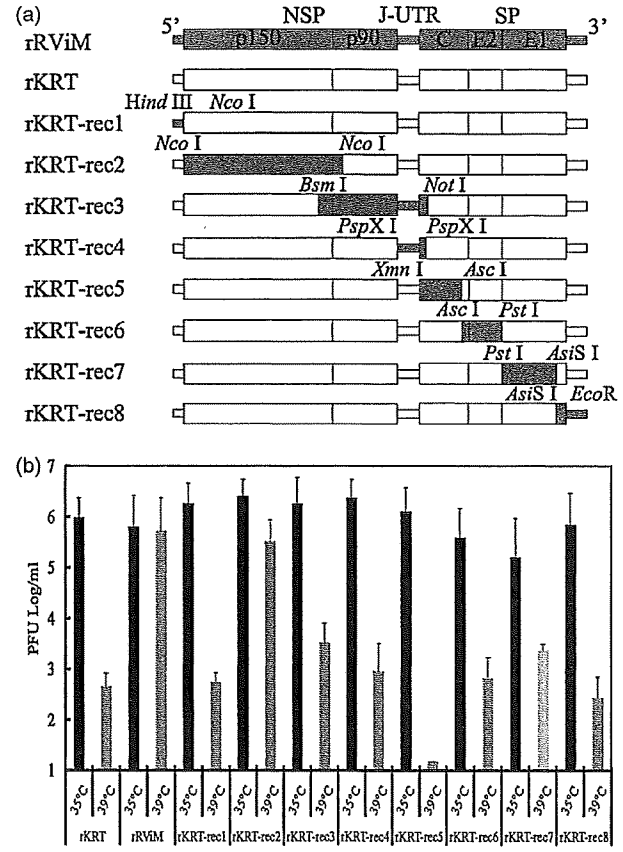

Fig. 3. Construction of a series of recombinant viruses based on rKRT and growth at 35 and 39 °C. (a) Construction of rKRT-rec1–8 based on the rKRT. The genomic structure of RV is indicated in the panel. The broad boxes demonstrate ORFs containing the NSP (p150 and p90) at the 5′ end and the SP (capsid, E2, and E1) at the 3′ end. Narrow boxes between two ORFs indicate untranslated regions (5′ UTR, J-UTR, and 3′ UTR). A series of viruses, rKRT-rec1–8, based on rKRT backbone were constructed by replacing the fragments of rKRT with those of rRViM after digestion with appropriate restriction enzymes. Fragments derived from rRViM are shown as gray bars and from the rKRT backbone, as open bars. (b) Infectivity of respective recombinant viruses at 35 and 39 °C. RK13 cells were infected at a MOI of 0.01. The culture medium was harvested at 96 hpi, and the infective titer was measured. The black columns indicate the infective titers at 35 °C and the gray columns, those at 39 °C. The average infective titers in three independent experiments are shown and the error bar indicates ±SD.

Nde I (gp 1872), Nhe I (gp 2803), Bsm I (gp 3243), and Eco RV (gp 4213), shown in Fig. 5.

There were three nucleotide substitutions with two amino acid changes [G and D at amino acid (a.a.) position 1007, H and Y at 1042] in the Nhe I-Bsm I region of p150 between the KRT strain and wild-type RVi/Matsue.JPN/68 strain. Nucleotide mutations were introduced either independently or in combination into pKRT by PCR amplification with the GeneTailor™ Site-Directed Mutagenesis System (Invitrogen), using as a forward primer, 5′-GCCGGCGaCCCGGGCCGACCGGCTCAGCG-3′ (gp 3053–3082), and as a reverse primer, 5′-GGTCGGCCCGGGtCGCCGGCGGGGCAAGAT-3′ (gp 3043–3072), for the mutation of G to A at gp 3060 (G to D at a.a. position 1007) and 5′-GGTGCGAACTCTGCCGGtAt-ACGCGCGTCA-3′ (gp 3147–3176) and 5′-CCGGCAGAGTTCGCACCC-CTGGCATCCGC-3′ (gp 3135–3163) for the mutations of C to T at gp 3164 and C to T at gp 3166 (H to Y at a.a. position 1042, nucleotide mutations indicated in lower case). The three point-mutated viruses were designated G1007D, H1042Y and G1007D-H1042Y, respectively (Fig. 6). Two recombinant viruses H1042Y-RViM p90 and H1042Y-RViM SP were constructed, using the restriction enzyme sites Bsm I (gp 3243), Not I (gp 6623), Xmn I (gp 6514), and Eco RI (3′ end) as shown in Fig. 7.

2.5. Recovery of clone viruses from infectious cDNA clones of RV

The full-length viral genomic RNA was synthesized from the infectious cDNA clones with the mMESSAGE mMACHINE T7 kit (Applied Biosystems) following the instruction manual. Vero and RK13 cells were prepared at 8.0×10^5 cells/well in 6-well Plates 24 h before RNA transfection. After the cells were washed with 2.0 ml of OPTI-MEM, RNA transfection was carried out with a mixture of 12.5 μg of synthesized RNA and 15.0 μl of DMRIE-C (Invitrogen) in 1.0 ml of OPTI-MEM. After incubation at 35 °C for 4 h, the mixture was removed and replaced with 2.0 ml of MEM containing 5% FBS. For calculating the recovery kinetics of clone viruses, a 100-μl aliquot of culture fluid was harvested every 24 h until 120 h after transfection. The kinetics of infectious clone viruses was monitored with a plaque assay.

2.6. Analysis of temperature sensitivity

Monolayers of RK13 cells in 6-well plates were infected at a multiplicity of infection (MOI) of 0.01. After adsorption, each well was washed twice with 2.0 ml of PBS and replaced with 2.0 ml of MEM

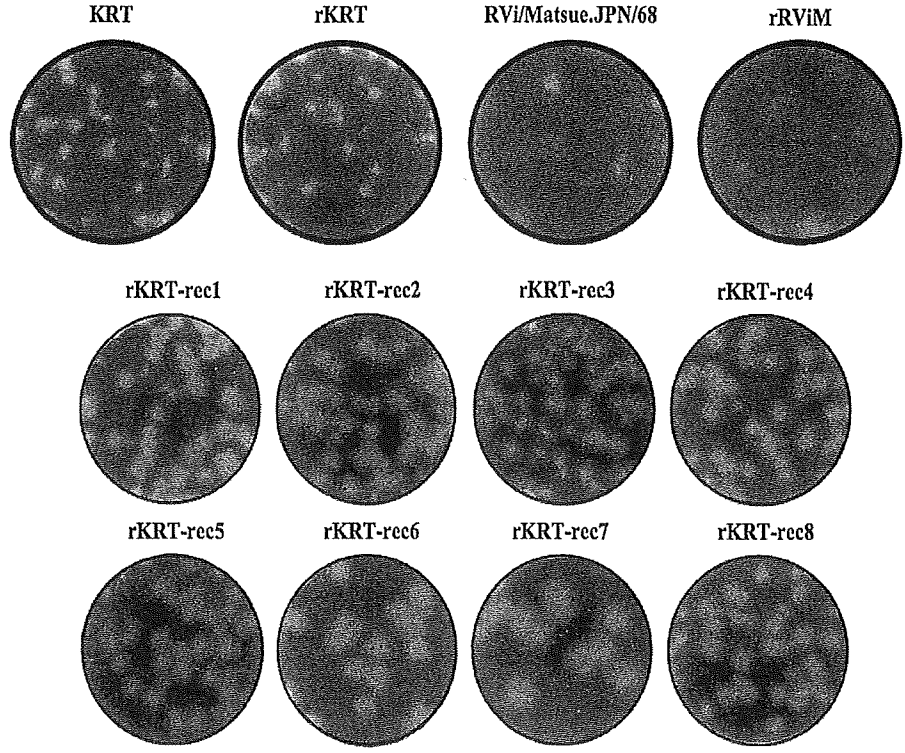

Fig. 4. The plaque morphology of rKRT, rRViM, the original KRT and RVi/Matsue.JPN/68, and the chimeric viruses. Plaques were visualized by fixation with a staining solution containing crystal violet.

containing 5% FBS and antibiotics. The plates were incubated at 35 or 39 °C in a 5% CO_2 incubator, and the culture medium was collected at 24, 48, 72, 96, or 120 h post-infection (hpi). The infective titer of the medium was determined by the plaque assay.

2.7. Viral titration by plaque assay

Monolayers of RK13 cells in 6-well plates were infected with 10-fold serial dilutions of samples. The inoculum was removed after 1 h of contact at room temperature and replaced with 3.0 ml of MEM containing 2% FBS, 40 μg/ml of DEAE dextran, 0.07% sodium bicarbonate, 0.7% agarose, penicillin 100 U/ml and streptomycin 100 U/ml. The plates were incubated at 35 °C in a 5% CO_2 incubator. On day 7 post-infection, plaques were visualized by staining with PBS containing 0.1% crystal violet and 4% formalin [9,14,15].

2.8. Nucleotide sequence accession numbers

The entire sequences of the KRT vaccine strain and wild-type RVi/Matsue.JPN/68 strain were submitted to the GenBank database with accession numbers AB222608 and AB222609, respectively.

3. Results

3.1. Identification of the full-length genome sequence of the KRT vaccine strain and wild-type RVi/Matsue.JPN/68 strain

The live attenuated rubella vaccine KRT was developed by passaging a wild-type rubella virus in rabbit cells. It has been reported that the progenitor wild-type virus of the KRT strain was isolated from a patient with rubella in Matsue city, Japan in 1968 [6]. Although the progenitor was not available, the RVi/Matsue.JPN/68 strain was isolated in the same city in the same year. Consequently, RVi/Matsue.JPN/68 was used a reference for the wild-type of the KRT strain in this study. KRT has a temperature sensitivity (*ts*) phenotype, while the wild-type strains have no temperature sensitivity (non-*ts*) phenotype. The *ts* phenotype of KRT means restricted viral replication at 39 °C [7]. Although little is known about the mechanism of *ts*, it is widely recognized that the phenotype relates to viral attenuation [7,16–19]. The genome of both the KRT and RVi/Matsue.JPN/68 strains was 9762 nt in length. Both genomes consisted of a 40-nt 5′ UTR, 6348-nt NSP, 123-nt J-UTR, 3189-nt SP, and 62-nt 3′ UTR, and were classified into the clade Ia. At the nucleotide level, the entire genomes of the two strains varied by 2.38% (232/9762 nt), while at the amino acid level, they varied by 1.04% (33/3179 a.a.). Tables 1 and 2 show the nucleotide and amino acid differences between the KRT and RVi/Matsue.JPN/68 viruses. Nucleotide differences in the E2 region were highest at 3.19% (27/846 nt) with 2.84% (8/282 a.a.) of amino acids differing. In each region 1.77–3.19% of nucleotides differed and 0.12–2.84% of amino acids differed.

3.2. Construction and characterization of infectious cDNA clones of KRT and RVi/Matsue.JPN/68

Infectious cDNA clones were constructed from the KRT and RVi/Matsue.JPN/68 viruses (Fig. 1). The amplified cDNA fragments were cloned into pUC18 and these clones were assembled into a full-length cDNA clone by using appropriate restriction enzymes. To synthesize the viral RNA, the T7 promoter sequence and a polyA tract were introduced into the full-length cDNA clone. The infectious cDNA clones of KRT and RVi/Matsue.JPN/68 were named pKRT and pRViM, respectively.

Clone viruses of rKRT and rRViM were obtained after transfection of RNA synthesized *in vitro* from the infectious cDNA clones of RVs. To monitor the kinetics of recovery after the transfection of RNA into Vero and RK13 cells, aliquots were harvested and viral titers were determined by plaque assay (Fig. 2a). Maximum infec-

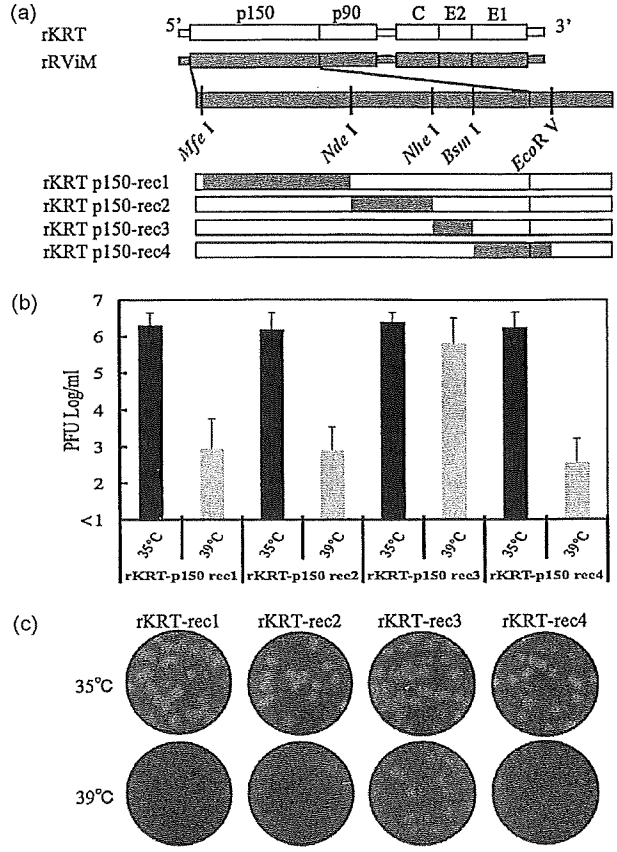

Fig. 5. Construction and characteristics of the recombinant viruses rKRT-p150 rec1~4. (a) Construction of a series of recombinant viruses in the p150 region based on rKRT and rRViM. Gray bars represent the regions derived from rRViM and open bars, those from rKRT. Four chimeric viruses were generated by introducing a part of the p150 region of rRViM into rKRT using appropriate restriction enzyme sites. (b) Infectivity of recombinant viruses. RK13 cells were infected with the rKRT p150 chimeric viruses. The black and gray columns show the infective titers at 35 °C and 39 °C, respectively. The average infective titer in three independent experiments is shown and the error bar indicates ±SD. (c) Plaque assay. Panels at 35 °C demonstrate the results of the plaque assay in 10^{-4} dilutions and panels at 39 °C, these in 10^{-3} dilutions.

tivity of the infectious clone virus (rKRT), 1.0×10^6 PFU/ml, was obtained in Vero cells 96 h after transfection, while the peak of infectivity in RK13 cells reached 2.0×10^5 PFU/ml 72 h after transfection. Thereafter, the clone viruses were recovered at 96 h after transfection in Vero cells. The viruses were propagated within two passages in Vero cells and used for further experiments.

It has been reported that KRT had the *ts* phenotype but the wild-type strain did not [7]. The growth of KRT at 39 °C decreased to 1/1000 of that at 35 °C. The infectivity of RVi/Matsue.JPN/68 at 39 °C was approximately 1/5 of that at 35 °C. The growth patterns of the recombinant viruses, rKRT and rRViM, were similar to those observed for the original viruses (Fig. 2b and c).

The clone viruses were efficiently recovered from the infectious cDNA clone of the KRT vaccine strain and of the wild-type RVi/Matsue.JPN/68 strain. The clones retained the characteristics of the original viruses *in vitro*.

3.3. Construction of chimeric viruses and properties of viral replication at 35 and 39 °C

In order to determine the genomic region responsible for the *ts* phenotype of the KRT vaccine strain, eight recombinant chimeric viruses were constructed based on rKRT, replacing parts of the KRT

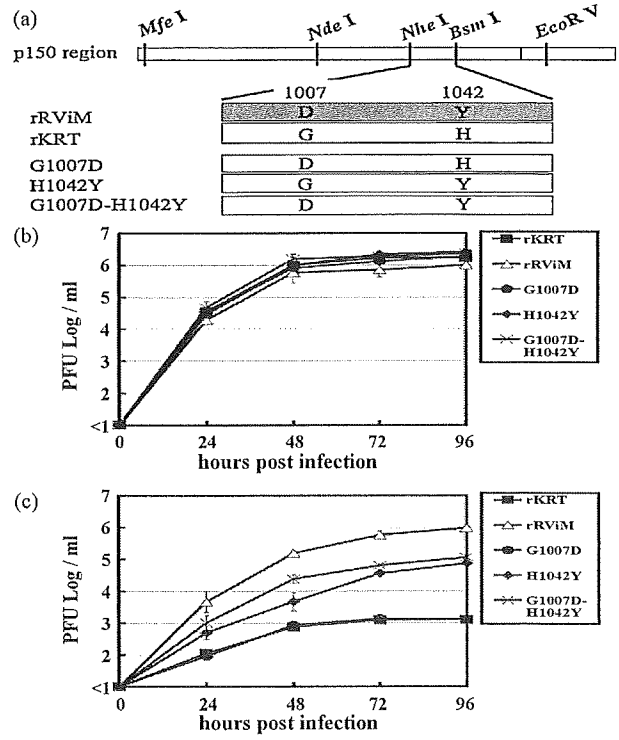

Fig. 6. Growth kinetics of point-mutated RVs at 35 and 39 °C. (a) Amino acid differences in the Nhe I-Bsm I region of p150 between KRT and RVi/Matsue.JPN/68 and construction of mutated viruses. Mutated viruses were generated by introducing the amino acid residues of rRViM into rKRT. Three constructs, G1007D, H1042Y, and G1007D-H1042Y, are illustrated. (b) Growth kinetics of the mutated viruses at 35 °C. The results show the average for three independent experiments and the error bar indicates the ±SD. (c) Growth kinetics of mutated viruses at 39 °C.

genome with the corresponding sequence of RVi/Matsue.JPN/68 (Fig. 3a). Suitable restriction enzymes were used in order to exchange the fragments of individual proteins and UTR regions between the KRT and RVi/Matsue.JPN/68 viruses. For example, rec2 was constructed by exchanging the amino acids in the p150 gene without exchanging those in the p90 gene.

To identify the region responsible for the *ts* phenotype, we examined the growth properties of the recombinant chimeric viruses (rKRT-rec1–8), rKRT, and rRViM, in RK13 cells at 35 and 39 °C. As shown in Fig. 3b, the rKRT-rec1–8 chimeric viruses, except rec2, demonstrated a reduction in growth at 39 °C and the difference in infective titer at 39 °C versus 35 °C varied from 1/100 to 1/10000, similar to that for rKRT. However, rKRT-rec2 grew well at 39 °C in comparison with the other recombinant viruses, its infectivity being 1/10 that at 35 °C. We also obtained complementary results with recombinant chimeric viruses based on rRViM (data not shown). Replacement of the p150 of rKRT with that of rRViM abrogated the *ts* phenotype and the introduction of the p150 of rKRT into rRViM reduced the growth at 39 °C with less efficiency. Thus, the *ts* phenotype of KRT depends on the p150 region.

The morphology of plaques was reported to differ among strains [9,10,20,21], and such a difference between KRT and RVi/Matsue.JPN/68 is shown in Fig. 4. KRT produced mainly small plaques with sharp and clear margins, while RVi/Matsue.JPN/68 generated mainly large plaques with vague and opaque margins. The clone viruses, rKRT and rRViM, exhibited the same plaque morphology as the original viruses. In addition, the plaques differed in size among the recombinant chimeric viruses. Among a series of rKRT-recs, rKRT-rec1, 2, 3, 4, 5, and 8 showed similar plaques, while rKRT-rec6 and rec7 generated apparently large plaques with clear and sharp margins. These results suggested that the envelope

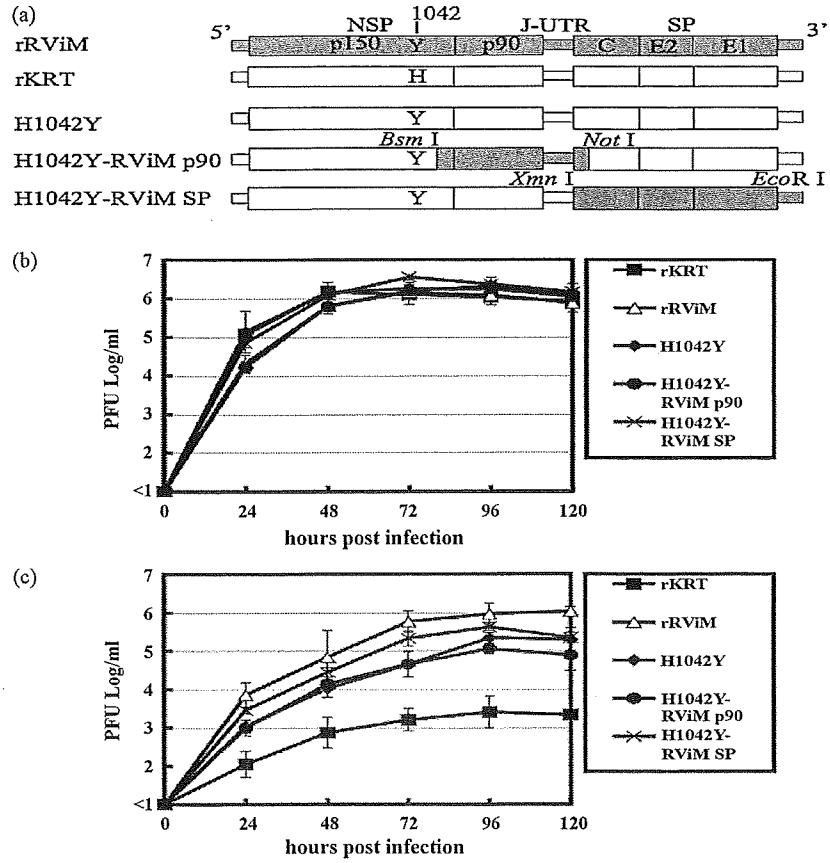

Fig. 7. Additive effect of other genomic regions on temperature sensitivity. (a) Construction of recombinant viruses (H1042Y-RViM p90 and H1042Y-RViM SP). The gray bars represent the fragments derived from rRViM and the white bars are those from rKRT. The recombinant viruses H1042Y-RViM p90 and H1042Y-RViM SP having the p90 and SP of rRViM together with the amino acid substitution H1042Y were generated, using the appropriate restriction enzyme sites (Bsm I, Not I, Xmn I, and Eco RI). (b) Growth kinetics of the recombinant viruses at 35 °C. The infective titer is shown as the average for three independent experiments and the error bar indicates ±SD. (c) Growth kinetics of recombinant viruses at 39 °C.

proteins, E1 and E2, of RVi/Matsue.JPN/68 were relevant to large plaques.

3.4. Identification of the amino acid residue in p150 responsible for the temperature sensitivity

The chimeric viruses altered in the p150 region (rKRT-rec2) varied in *ts* phenotype. Since there were 15 amino acid differences in the p150 region between the two strains, four recombinant viruses (rKRT p150-rec1–4) were generated based on rKRT, replacing the fragments in the p150 region between rKRT and rRViM (Fig. 5a). The growth of the rKRT p150-recs was investigated at 35 and 39 °C in RK13 cells and the results are shown in Fig. 5b and c. All rKRT p150-recs showed similar infectivity, over 10^6 PFU/ml at 35 °C, but the infective titers of p150-rec1, 2, and 4 were less than 10^3 PFU/ml at 39 °C. Only rKRT p150-rec3 demonstrated efficient growth, over 10^5 PFU/ml, at 39 °C. rKRT p150-rec3 consisted of the fragment between Nhe I and Bsm I in the p150 region of rRViM which seemed to be relevant to the *ts* phenotype of KRT. There were two amino acid differences in the Nhe I-Bsm I region of p150 between the two strains, at positions 1007 and 1042 (see Table 2). The amino acid at position 1007 of p150 was changed from aspartic acid (D) in RVi/Matsue.JPN/68 to glycine (G) in KRT. The other at position 1042 was changed from tyrosine (Y) in RVi/Matsue.JPN/68 to histidine (H) in KRT. In order to decide the amino acid residue(s) responsible for the *ts* phenotype, three mutated viruses, G1007D, H1042Y, and G1007D-H1042Y, containing a substitution at position 1007, 1042, or both of RVi/Matsue.JPN/68, were constructed (Fig. 6a). The growth kinetics at 35 and 39 °C are shown in Fig. 6b and c. G1007D, H1042Y, and G1007D-H1042Y grew well at 35 °C with similar titers, but G1007D showed poor growth similar to rKRT at 39 °C. Whereas, H1042Y and G1007D-H1042Y showed more efficient growth at 39 °C with 100-fold higher titers than rKRT. These results indicated that the histidine at position 1042 of p150 was responsible for the *ts* phenotype of the KRT.

3.5. Additive effect of other regions on the ts

The histidine at position 1042 of p150 was considered to be responsible for the *ts* phenotype of KRT, but the growth kinetics of H1042Y and G1007D-H1042Y at 39 °C did not completely match that of rRViM. The peak infective titers of those viruses at 39 °C were about 1/10 lower than those of rRViM (Fig. 6c). There remained the possibility that other gene(s) influenced the growth properties at restrictive temperatures in relation with the tyrosine at position 1042, thus we examined the additive effect of other gene(s) to allow better growth at 39 °C. We constructed two additional recombinant viruses having p90 or structural proteins (SP) including capsid, E2, and E1 of RVi/Matsue.JPN/68 together with the substitution H1042Y (Fig. 7a). There was no difference in growth among the recombinant viruses (H1042Y, H1042Y-RViM p90 and H1042Y-RViM SP) at 35 °C. The growth kinetics of H1042Y and H1042Y-RViM p90 showed a very similar pattern at 39 °C, while the growth of H1042Y-RViM SP was greater than that of H1042Y, the maximum titer (at 96 hpi) approaching that of rRViM. These results suggested that the p90 of RVi/Matsue.JPN/68 had no additive effect with the

tyrosine at position 1042 of p150 on the growth at a restrictive temperature, whereas the SP region of RVi/Matsue.JPN/68 did have an additive effect.

4. Discussion

For the prevention of CRS and rubella epidemics, live attenuated rubella vaccines have been used in vaccination programs in many countries. Although these vaccines have high efficacy and a low incidence of adverse reactions, their attenuation mechanism is not well understood. A few studies reported replication properties, plaque morphology and cell tropism of the RA27/3 and Cendehill vaccine strains, leading to some insight into the attenuation. RA27/3 has been used widely for vaccination programs and was reported to have unique characteristics *in vitro*, probably related to the attenuation, in comparison with the wild-type virus (Therien strain). RA27/3 formed smaller plaques with lower growth than Therien due to mutations in the 5′ UTR, the protease motif of p150, and the capsid region [8–10,22]. The Cendehill strain is known to cause acute arthritis at a very low incidence, a phenomenon that seems to correlate with a drastic reduction in growth in synovial cells compared with the wild-type virus [8,23]. Chantler et al. [20] also reported differences in plaque morphology and growth properties among rubella virus strains. All Japanese vaccines, RA27/3, and Cendehill, exhibit the *ts* phenotype, which is probably linked with immunogenic markers in rabbits and guinea pigs [7,16,20,24]. In some single positive strand RNA viruses, such as *Togaviridae* and *Flaviridae* family viruses: sindbis virus, semiliki forest virus, tick-borne encephalitis virus and dengue virus, the *ts* phenotype was shown to be related to attenuation in animal models [17,19,25,26]. Therefore, the *ts* phenotype of the KRT vaccine strain was considered a biological marker of attenuation.

In this study, the biological characteristics of the KRT vaccine were compared with those of RVi/Matsue.JPN/68, which was isolated in the same city and year as the KRT progenitor. The genomes of both strains consisted of 9762 nt and there were 232 nucleotide differences with 33 amino acid changes between the two. These differences were more frequent than those between the TO-336 vaccine and TO-336 progenitor wild-type strains: Kakizawa et al. [27] reported that the two genomic sequences differed at 21 nt with 10 amino acid changes. Although KRT and RVi/Matsue.JPN/68 belong to genotype Ia of rubella virus, consisting of the RA27/3, Cendehill, and TO-336 vaccine strains, and other wild-type strains, none of the mutations observed in KRT was common to those vaccine strains [8,27–32]. Thus, the region(s) responsible for the *ts* phenotype would differ among vaccine strains.

In order to investigate the genetic determinant(s) of the *ts* phenotype in KRT, we developed a RG system with KRT and RVi/Matsue.JPN/68. There were significant biological differences between KRT and RVi/Matsue.JPN/68. The clone virus, rKRT, and its original virus produced small plaques with sharp and clear margins, while rRViM and its original virus produced large plaques with vague and opaque margins. rKRT, rRViM, and their original viruses grew well at 35 °C without any changes in growth kinetics, but the growth kinetics differed significantly at 39 °C. The clones, rKRT and rRViM, showed the same biological characteristics as the original viruses.

A series of recombinant viruses (rKRT-rec1–8) based on rKRT and rRViM were generated, to investigate the contribution of individual regions of the genome to the *ts* phenotype of KRT. rKRT-rec2 (replacement of the p150 region) differed in phenotype from the original virus, however, the others showed similar growth properties to the parental viruses. We also found that some parts of the genome affected the morphology of plaques in the process of detecting the region responsible for the *ts* phenotype. The difference in the morphology of the plaques between the two strains was determined with crystal violet staining. Crystal violet stains living cells, and therefore plaque morphology, e.g. vague, opaque, clear and sharp may reflect apoptotic cell distribution, probably related to the difference in the regulation of viral replication and cytopathic effect between the two strains. Moreover, the introduction of E1 and E2 proteins of RVi/Matsue.JPN/68 changed the small plaques of rKRT to large ones. E1 and E2 having N-linked glycosylation sites (Asn-X-Ser/Thr) form heterodimers and compose the viral particle. After the formation of the heterodimer, N-linked glycosylation occurred during transport to the budding site. E1 and E2 play a key role in budding at the plasma membrane of infected cells, and the attachment to and entry of an uninfected cell occur through the fusion activity of these proteins [33,34]. It has also reported that the formation of the heterodimer and N-linked glycosylation influence infectivity and membrane fusion activity [35–41]. There were 13 amino acid differences in the E1 and E2 proteins, one of which was in the predicted N-linked glycosylation site at amino acid position of the E1 region (Table 2). This difference causes the absence of one predicted N-linked glycosylation site in E1 of KRT. As a result, two predicted N-linked glycosylation sites exist in the E1 region of KRT and three sites in that of RVi/Matsue.JPN/68, and a difference in the molecular weight of E1 between the two strains was observed by Western blotting (data not shown). The recombination of E1 and E2 (rKRT-rec6 and rec7) obviously altered plaque size. Thus, the large plaques of RVi/Matsue.JPN/68 might suggest an efficient expansion of infection *in vitro*. The different numbers of predicted N-linked glycosylation sites and amino acid changes may be involved in the membrane fusion activity and conformational change of those proteins leading to an influence on viral spread from cell to cell. Further investigation is required to clarify whether the characteristic morphology of plaques is correlated with the attenuation process.

There are 15 amino acid differences in the p150 region between the KRT and RVi/Matsue.JPN/68 strains. Four recombinant viruses (rKRT p150-rec1–4) and mutated viruses (G1007D, H1042Y, and G1007D-H1042Y) demonstrated that the histidine at position 1042 was critical for the *ts* phenotype of KRT. Although the growth of the H1042Y mutant was 100-fold greater than that of rKRT at 39 °C, the peak infective titer was 1/10 that of rRViM. Therefore, the additive effect of the other region(s) on growth at 39 °C was investigated, together with H1042Y. Although the p90 region of RVi/Matsue.JPN/68 had no additive effect on the *ts* phenotype, SP (structural proteins: capsid, E2, and E1) exhibited an additive effect on replication at 39 °C. The reduction in peak titer of the H1042Y mutant may be due to the differences in genetic background between KRT and RVi/Matsue.JPN/68.

In this study, we did not evaluate the effect of this histidine on p150 and the defective viral life cycle. The p150 region encodes a methyltransferase motif having a role in the capping of viral RNA and a cysteine protease domain that cleaves a precursor p200 polyprotein to p150 and p90 proteins as functional units. Balistreri et al. [42] reported that variation in the *ts* phenotype of Semliki forest virus having mutations in the protease domain indicated a great reduction of protease activity compared to the wild-type virus at a restricted temperature. The change in the *ts* phenotype of Sindbis virus with mutations in the protease domain reduced subgenomic RNA synthesis [43–46]. These reports provided new insights into the mechanism of the *ts* of KRT. Because the histidine at position 1042 is located in the protease domain, it may cause defects in NSP processing or viral RNA replication; synthesis of negative strand RNA (cRNA), subgenomic RNA, and progenitor genomic RNA.

Acknowledgements

We would like to thank F. Momose, PhD and Y. Morikawa, PhD for their matchless technical competence and thoughtful advice.

References

[1] Chantler J, Wolinsky JS, Tingle A. Rubella virus. In: Knipe DM, Howley PM, editors. Fields virology. 4th edition Philadelphia, PA: Lippincott Williams & Wilkins; 2001. p. 963–90.
[2] Frey TK. Molecular biology of rubella virus. Adv Virus Res 1994;44:69–160.
[3] Banatvala JE, Brown DW. Rubella. Lancet 2004;363(9415):1127–37.
[4] WHO. Rubella vaccines. WHO position paper. Wkly Epidemiol Rec 2000.
[5] Plotkin SA. Rubella eradication. Vaccine 2001;19(25–26):3311–9.
[6] Shishido A, Ohtawara M. Development of attenuated rubella virus vaccines in Japan. Jpn J Med Sci Biol 1976;29(October (5)):227–53.
[7] Ohtawara M, Kobune F, Umino Y, Sugiura A. Inability of Japanese rubella vaccines to induce antibody response in rabbits is due to growth restriction at 39 degrees C. Arch Virol 1985;83(3–4):217–27.
[8] Lund KD, Chantler JK. Mapping of genetic determinants of rubella virus associated with growth in joint tissue. J Virol 2000;74(January (2)):796–804.
[9] Pugachev KV, Abernathy ES, Frey TK. Improvement of the specific infectivity of the rubella virus (RUB) infectious clone: determinants of cytopathogenicity induced by RUB map to the nonstructural proteins. J Virol 1997;71(January (1)):562–8.
[10] Pugachev KV, Galinski MS, Frey TK. Infectious cDNA clone of the RA27/3 vaccine strain of Rubella virus. Virology 2000;273(1):189–97.
[11] Tzeng WP, Frey TK. Complementation of a deletion in the rubella virus p150 nonstructural protein by the viral capsid protein. J Virol 2003;77(September (17)):9502–10.
[12] Yao J, Gillam S. Mutational analysis, using a full-length rubella virus cDNA clone, of rubella virus E1 transmembrane and cytoplasmic domains required for virus release. J Virol 1999;73(June (6)):4622–30.
[13] Wang CY, Dominguez G, Frey TK. Construction of rubella virus genome-length cDNA clones and synthesis of infectious RNA transcripts. J Virol 1994;68(June (6)):3550–7.
[14] Fogel A, Plotkin SA. Markers of rubella virus strains in RK13 cell culture. J Virol 1969;3(February (2)):157–63.
[15] Umino Y. Improved potency assay of rubella vaccine: parameters for plaque formation. J Virol Methods 1995;51(February (2–3)):317–28.
[16] Plotkin SA, Cornfeld D, Ingalls TH. Studies of immunization with living rubella virus. Trials in children with a strain cultured from an aborted fetus. Am J Dis Child 1965;110(October (4)):381–9.
[17] Schluter B, Bellomy B, Brown A. Pathogenesis of temperature-sensitive mutants of sindbis virus in the embryonated egg. I. Characterization and kinetics of viral multiplication. Infect Immun 1974;9(January (1)):68–75.
[18] Krieger JN, Scherer WF, Wiebe ME, Pancake BA, Harsanyi ZP. A hamster-attenuated, temperature-sensitive mutant of Venezuelan encephalitis virus. Infect Immun 1979;25(September (3)):873–9.
[19] Ehrengruber MU, Renggli M, Raineteau O, Hennou S, Vaha-Koskela MJ, Hinkkanen AE, et al. Semliki Forest virus A7(74) transduces hippocampal neurons and glial cells in a temperature-dependent dual manner. J Neurovirol 2003;9(February (1)):16–28.
[20] Chantler JK, Lund KD, Miki NP, Berkowitz CA, Tai G. Characterization of rubella virus strain differences associated with attenuation. Intervirology 1993;36(4):225–36.
[21] Kouri G, Aguilera A, Rodriguez P, Korolev M. A study of microfoci and inclusion bodies produced by rubella virus in the RK-13 cell line. J Gen Virol 1974;22(January (1)):73–80.
[22] Pugachev KV, Frey TK. Effects of defined mutations in the 5′ nontranslated region of rubella virus genomic RNA on virus viability and macromolecule synthesis. J Virol 1998;72(January (1)):641–50.
[23] Miki NP, Chantler JK. Differential ability of wild-type and vaccine strains of rubella virus to replicate and persist in human joint tissue. Clin Exp Rheumatol 1992;10(January-February (1)):3–12.
[24] Linnemann Jr CC, Hutchinson L, Rotte TC, Hegg ME, Schiff GM. Stability of the rabbit immunogenic marker of RA 27-3 rubella vaccine virus after human passage. Infect Immun 1974;9(March (3)):547–9.
[25] Rumyantsev AA, Murphy BR, Pletnev AG. A tick-borne Langat virus mutant that is temperature sensitive and host range restricted in neuroblastoma cells and lacks neuroinvasiveness for immunodeficient mice. J Virol 2006;80(February (3)):1427–39.
[26] Blaney Jr JE, Johnson DH, Firestone CY, Hanson CT, Murphy BR, Whitehead SS. Chemical mutagenesis of dengue virus type 4 yields mutant viruses which are temperature sensitive in vero cells or human liver cells and attenuated in mice. J Virol 2001;75(October (20)):9731–40.
[27] Kakizawa J, Nitta Y, Yamashita T, Ushijima H, Katow S. Mutations of rubella virus vaccine TO-336 strain occurred in the attenuation process of wild progenitor virus. Vaccine 2001;19(April (20–22)):2793–802.
[28] Zhou Y, Ushijima H, Frey TK. Genomic analysis of diverse rubella virus genotypes. J Gen Virol 2007;88(March (Pt 3)):932–41.
[29] Frey TK, Abernathy ES, Bosma TJ, Starkey WG, Corbett KM, Best JM, et al. Molecular analysis of rubella virus epidemiology across three continents, North America, Europe, and Asia, 1961–1997. J Infect Dis 1998;178(September (3)):642–50.
[30] Pugachev KV, Abernathy ES, Frey TK. Genomic sequence of the RA27/3 vaccine strain of rubella virus. Arch Virol 1997;142(6):1165–80.
[31] Dominguez G, Wang CY, Frey TK. Sequence of the genome RNA of rubella virus: evidence for genetic rearrangement during togavirus evolution. Virology 1990;177(July (1)):225–38.
[32] Clarke DM, Loo TW, Hui I, Chong P, Gillam S. Nucleotide sequence and in vitro expression of rubella virus 24S subgenomic messenger RNA encoding the structural proteins E1, E2 and C. Nucleic Acids Res 1987;15(April (7)):3041–57.
[33] Doms RW, Lamb RA, Rose JK, Helenius A. Folding and assembly of viral membrane proteins. Virology 1993;193(April (2)):545–62.
[34] Anthony RP, Brown DT. Protein–protein interactions in an alphavirus membrane. J Virol 1991;65(March (3)):1187–94.
[35] Ramanujam M, Hofmann J, Nakhasi HL, Atreya CD. Effect of site-directed asparagine to isoleucine substitutions at the N-linked E1 glycosylation sites on rubella virus viability. Virus Res 2001;81(December (1–2)):151–6.
[36] Law LM, Duncan R, Esmaili A, Nakhasi HL, Hobman TC. Rubella virus E2 signal peptide is required for perinuclear localization of capsid protein and virus assembly. J Virol 2001;75(February (4)):1978–83.
[37] Yao J, Gillam S. A single-amino-acid substitution of a tyrosine residue in the rubella virus E1 cytoplasmic domain blocks virus release. J Virol 2000;74(April (7)):3029–36.
[38] Qiu Z, Tufaro F, Gillam S. The influence of N-linked glycosylation on the antigenicity and immunogenicity of rubella virus E1 glycoprotein. Virology 1992;190(October (2)):876–81.
[39] Qiu Z, Yao J, Cao H, Gillam S. Mutations in the E1 hydrophobic domain of rubella virus impair virus infectivity but not virus assembly. J Virol 2000;74(July (14)):6637–42.
[40] Garbutt M, Law LM, Chan H, Hobman TC. Role of rubella virus glycoprotein domains in assembly of virus-like particles. J Virol 1999;73(May (5)):3524–33.
[41] Yang D, Hwang D, Qiu Z, Gillam S. Effects of mutations in the rubella virus E1 glycoprotein on E1–E2 interaction and membrane fusion activity. J Virol 1998;72(November (11)):8747–55.
[42] Balistreri G, Caldentey J, Kaariainen L, Ahola T. Enzymatic defects of the nsP2 proteins of Semliki Forest virus temperature-sensitive mutants. J Virol 2007;81(March (6)):2849–60.
[43] Lulla V, Merits A, Sarin P, Kaariainen L, Keranen S, Ahola T. Identification of mutations causing temperature-sensitive defects in Semliki Forest virus RNA synthesis. J Virol 2006;80(March (6)):3108–11.
[44] Suopanki J, Sawicki DL, Sawicki SG, Kaariainen L. Regulation of alphavirus 26S mRNA transcription by replicase component nsP2. J Gen Virol 1998;79(February (Pt 2)):309–19.
[45] De I, Sawicki SG, Sawicki DL. Sindbis virus RNA-negative mutants that fail to convert from minus-strand to plus-strand synthesis: role of the nsP2 protein. J Virol 1996;70(May (5)):2706–19.
[46] Hahn YS, Strauss EG, Strauss JH, Rice CM, Levis R, Huang HV. Mapping of RNA-temperature-sensitive mutants of Sindbis virus: assignment of complementation groups A, B, and G to nonstructural proteins Production of infectious RNA transcripts from Sindbis virus cDNA clones: mapping of lethal mutations, rescue of a temperature-sensitive marker, and in vitro mutagenesis to generate defined mutants. J Virol 1989;63(7):3142–50.

Journal of Medical Virology 81:1094–1101 (2009)

Modified Adult Measles in Outbreaks in Japan, 2007–2008

Makoto Nagai,[1] Ji Yi Xin,[2] Naoko Yoshida,[3] Akiko Miyata,[4] Motoko Fujino,[5] Toshiaki Ihara,[6] Tetsushi Yoshikawa,[7] Yoshizo Asano,[7] and Tetsuo Nakayama[8]*

[1]*Department of Pediatrics, Tokyo Medical College, Tokyo, Japan*
[2]*China CDC, National Laboratory for Measles, National Institute for Viral Disease Control and Prevention, Beijing, China*
[3]*Department of Pediatrics, Tachikawa Kyousai Hospital, Tachikawa, Japan*
[4]*Miyata Pediatric Clinic, Tachikawa, Tokyo, Japan*
[5]*Department of Pediatrics, Tokyo Saiseikai Central Hospital, Tokyo, Japan*
[6]*Department of Pediatrics, National Mie Hospital, Tsu, Mie, Japan*
[7]*Department of Pediatrics, School of Medicine, Fujita Health University, Toyoake, Aichi, Japan*
[8]*Laboratory of Viral Infection I, Kitasato Institute for Life Sciences, Shirokane, Minato-ku, Tokyo, Japan*

Different genotypes of C1, D3, D5, and H1 were isolated in outbreaks of 1984, 1987–1988, 1991–1993, and 2001, respectively, when the previous circulating genotype was replaced successively by a new genotype, through molecular studies of measles since 1984 in Japan. In March 2007, several patients with measles were observed in outpatient clinics, who were all young adolescents in high school and university students. The outbreak expanded subsequently throughout Japanese districts in May and is still ongoing in 2008. Reverse transcription loop-mediated isothermal amplification (RT-LAMP) was used to detect the measles genome from 18 clinical samples obtained from patients suspected of modified measles infection with a very mild febrile illness. The measles genome was detected in nine patients by reverse transcription polymerase chain reaction (RT-PCR) and in 12 patients by RT-LAMP. Six measles strains were isolated in the 2007–2008 outbreak and identified as the D5 genotype (MVi/Bangkok.THA/93 type) different from the D5 sub-cluster (MVi/Palau.BLA/93 type) isolated in 1990–2005. Similar Bangkok type D5 strains were isolated in Phnom Penh in 2002 and in Taiwan in 2003, suggesting that the D5 strains might have been introduced via South East Asia, rather than resulting from the accumulation of mutations in the D5 strains of 1990–2005. One D9 strain was isolated from a sporadic case in Aichi in 2006. There was no difference in the antigenicity of the D9 and D5 strains in comparison with the vaccine strain. Infrastructure of systematic laboratory-based surveillance system should be established in order to confirm measles virus infection in Japan. ***J. Med. Virol. 81:1094–1101, 2009.*** © 2009 Wiley-Liss, Inc.

KEY WORDS: measles virus; measles vaccine; modified measles; genotype; neutralization test antibody

INTRODUCTION

Measles is still a major killer among infants in developing countries, and the World Health Assembly endorsed a resolution to achieve the goal of reduction of measles deaths that occurred in 1999 by half by the end of 2005 [WHO, 2002]. WHO/UNICEF estimates indicated that global routine measles vaccination coverage increased from 72% in 2000 to 80% for the first dose in 2006 and that the number of measles-related deaths decreased from 873,000 in 1999 to 345,000 in 2005 and to 242,000 in 2006, and so the tentative goal for 2005 was achieved on schedule [WHO, 2002; CDC, 2007]. Indigenous outbreaks of measles were eliminated in the USA by the implementation of a two-dose measles–mumps–rubella trivalent vaccine (MMR) program and the sporadic cases reported in the USA were caused by importation from areas where measles is not yet controlled, such as Africa and Asian countries, including Japan [Rota et al., 1998, 2002; Strebel et al., 2004].

The contents of this article were presented at the 11th annual meeting of Japanese Society of Vaccinology, Yokohama, 2007.

Grant sponsor: Ministry of Education, Culture, Sports, Science and Technology of Japan (21st Century COE Program).

*Correspondence to: Tetsuo Nakayama, Laboratory of Viral Infection I, Kitasato Institute for Life Sciences, Shirokane 5-9-1, Minato-ku, Tokyo 108-8641, Japan.
E-mail: tetsuo-n@lisci.kitasato-u.ac.jp

Accepted 11 September 2008

DOI 10.1002/jmv.21372

Published online in Wiley InterScience (www.interscience.wiley.com)